
Ergodic variational flows

Zuheng Xu
University of British Columbia

Naitong Chen
University of British Columbia

Trevor Campbell
University of British Columbia

Abstract

This work presents a new class of variational family—*ergodic variational flows*—that not only enables tractable i.i.d. sampling and density evaluation, but also comes with MCMC-like convergence guarantees. Ergodic variational flows consist of a mixture of repeated applications of a measure-preserving and ergodic map to an initial reference distribution. We provide mild conditions under which the variational distribution converges weakly and in total variation to the target as the number of steps in the flow increases; this convergence holds regardless of the value of variational parameters, though different parameter values may result in faster or slower convergence. We develop an implementation of the flow family using Hamiltonian dynamics combined with deterministic momentum refreshment, including a tunable step size to optimize the trade-off between simulation fidelity and computational cost. Simulated and real data experiments provide an empirical verification of the convergence theory, and demonstrate that the method provides more reliable posterior approximations than several black-box normalizing flows, as well as samples of comparable quality to those obtained from state-of-the-art MCMC methods.

involves simulating a Markov chain whose stationary distribution is the Bayesian posterior distribution, and then treating the sequence of states as draws from the posterior. MCMC methods are supported by theory that guarantees that if one simulates the chain for long enough, Monte Carlo averages based on the sequence of states will converge to the exact posterior expectation of interest (e.g., Roberts and Rosenthal (2004)). This “exactness” property is quite compelling: regardless of how well one is able to tune the Markov chain, the method is guaranteed to eventually produce an accurate result given enough computation time. Nevertheless, it remains a challenge to assess and optimize the performance of MCMC in practice with a finite computational budget. One option is to use a Stein discrepancy (Gorham and Mackey, 2015; Liu et al., 2016; Chwialkowski et al., 2016; Gorham and Mackey, 2017; Anastasiou et al., 2021), which quantifies how well a set of MCMC samples approximates the posterior distribution. But standard Stein discrepancies are not reliable in the presence of multimodality (Wenliang and Kanagawa, 2020), are computationally expensive to estimate, and suffer from the curse of dimensionality, although recent work addresses the latter two issues to an extent (Huggins and Mackey, 2018; Gong et al., 2021). The other option is to use a traditional diagnostic, e.g., Gelman–Rubin (Gelman and Rubin, 1992; Brooks and Gelman, 1998), effective sample size (Gelman et al., 2013, p. 286), Geweke (1992), or others (Cowles and Carlin, 1996). These diagnostics detect mixing issues, but do not comprehensively quantify how well the MCMC samples approximate the posterior.

Variational inference (VI) (Jordan et al., 1999; Wainwright and Jordan, 2008; Blei et al., 2017) is an alternative to MCMC that does provide a straightforward quantification of posterior approximation error. In particular, VI involves approximating the posterior with a probability distribution—typically selected from a parametric family—that enables both i.i.d. sampling and density evaluation (Wainwright and Jordan, 2008; Rezende and Mohamed, 2015a; Ranganath et al., 2016; Papamakarios et al., 2021). Because one can take i.i.d. draws and evaluate the density, one can estimate the Kullback–Leibler (KL) divergence (Kullback and Leibler, 1951) to the posterior up to a constant. The ability to estimate this quantity, in turn, enables scalable tuning via straightforward stochastic gradient descent algorithms (Hoffman et al., 2013; Ranganath et al., 2014), optimally

1 Introduction

Bayesian statistical modelling and inference provides a principled approach to learning from data. However, for all but the simplest models, exact inference is not possible and computational approximations are required. A standard methodology for Bayesian inference is Markov chain Monte Carlo (MCMC) [Robert and Casella, 2004; Robert and Casella, 2011; Gelman et al., 2013, Ch. 11,12], which in-

mixed approximations (Jaakkola and Jordan, 1998; Gershman et al., 2012; Zobay, 2014; Guo et al., 2016; Wang, 2016; Miller et al., 2017; Locatello et al., 2018a,b; Campbell and Li, 2019), model selection (Corduneau and Bishop, 2001; Masa-aki, 2001; Constantinopoulos et al., 2006; Ormerod et al., 2017; Chérif-Abdellatif and Alquier, 2018; Tao et al., 2018), and more. However, VI typically does not possess the same “exactness regardless of tuning” that MCMC does. The optimal variational distribution is not usually equal to the posterior due to the use of a limited parametric variational family; and even if it were, one could not reliably find it in general due to nonconvexity of the KL objective (Xu and Campbell, 2022). Recent work addresses this problem by constructing variational families from parametrized Markov chains targeting the posterior. Many are related to annealed importance sampling (Salimans et al., 2015; Wolf et al., 2016; Geffner and Domke, 2021; Zhang et al., 2021; Thin et al., 2021a; Jankowiak and Phan, 2021); these methods introduce numerous auxiliary random variables and only have convergence guarantees in the limit of increasing dimension of the joint distribution. Those based on normalizing flows (Neal, 2005; Caterini et al., 2018; Chen et al., 2022) avoid the increase in dimension with flow length, but typically do not have guaranteed convergence to the target. Methods involving the final-state marginal of finite simulations of standard MCMC methods do not enable tractable density evaluation (Zhang and Hernández-Lobato, 2020).

In this work, we introduce a variational flow family—*ergodic variational flows*—that provide both MCMC-like convergence guarantees and tractable i.i.d. sampling and density evaluation (and hence ELBO estimates (Blei et al., 2017)). Ergodic variational flows are constructed by mixing over repeated application of a measure-preserving, ergodic map. Sampling using measure-preserving and ergodic maps, as well as mixed averages of pushforward distributions has appeared in past literature in various contexts (Aldous and Thorisson, 1993; Roberts and Rosenthal, 1997; Warren and Allen, 2018; Rotskoff and Vanden-Eijnden, 2019; Steeg and Galstyan, 2021; Thin et al., 2021b; Neklyudov and Welling, 2022), but our work is the first to construct a variational family and provide convergence theory. In particular, our main theoretical results (Theorems 3.1 and 3.2) provide mild conditions under which the ergodic variational distribution converges weakly and in total variation to the target as the number of flow steps increases. Since these results hold for any value of the variational parameter, we are assured that our method targets the right distribution regardless of the result of tuning—as in MCMC. But since we can take i.i.d. draws and evaluate the density, we have access to the ELBO, which enables variational parameter optimization. We present a practical instantiation of the general methodology based on Hamiltonian dynamics, with a discretization that can be tuned by maximizing the ELBO. Simulated and real data experiments verify the convergence of ergodic variational flows and showcase their performance in comparison

to the No-U-Turn sampler (NUTS) (Hoffman and Gelman, 2014), standard Hamiltonian Monte Carlo (HMC) (Neal, 2011), and several black-box normalizing flows (Rezende and Mohamed, 2015b; Dinh et al., 2017). Our results demonstrate a comparable output sample quality to NUTS, similar computational efficiency to HMC, and more reliable posterior approximations than standard normalizing flows.

2 Background

2.1 Variational inference with flows

Consider a set $\mathcal{X} \subseteq \mathbb{R}^d$ and a target probability distribution π on \mathcal{X} whose density with respect to the Lebesgue measure we denote $\pi(x)$ for $x \in \mathcal{X}$. In the setting of Bayesian inference, π is the posterior distribution that we aim to approximate, and we are only able to evaluate a function $p(x)$ such that $p(x) = Z \cdot \pi(x)$ for some unknown normalization constant $Z > 0$. Throughout, we will assume all distributions have densities with respect to the Lebesgue measure on \mathcal{X} , and will use the same symbol to denote a distribution and its density; it will be clear from context what is meant.

Variational inference involves approximating the target distribution π by minimizing the Kullback-Leibler (KL) divergence from π to members of a parametric family $\{q_\lambda : \lambda \in \Lambda\}$, $\Lambda \subseteq \mathbb{R}^p$, i.e.,

$$\begin{aligned} \lambda^* &= \arg \min_{\lambda \in \Lambda} D_{\text{KL}}(q_\lambda || \pi) \\ &= \arg \min_{\lambda \in \Lambda} \int q_\lambda(x) \log \frac{q_\lambda(x)}{p(x)} dx. \end{aligned} \quad (1)$$

The two objective functions in Eq. (1) differ only by the constant $\log Z$. In order to be able to optimize λ using standard techniques, the variational family q_λ , $\lambda \in \Lambda$ must enable both i.i.d. sampling and density evaluation. A common approach to constructing such a family is to pass draws from a simple reference distribution q_0 through a measurable function $T_\lambda : \mathcal{X} \rightarrow \mathcal{X}$; T_λ is often referred to as a *flow* when comprised of repeated composed functions (Tabak and Turner, 2013; Rezende and Mohamed, 2015a; Kobyzev et al., 2021). If T_λ is a *diffeomorphism*, i.e., differentiable and has a differentiable inverse, then we can express the density of $X = T_\lambda(Y)$, $Y \sim q_0$ as

$$\forall x \in \mathcal{X}, q_\lambda(x) = \frac{q_0(T_\lambda^{-1}(x))}{J_\lambda(T_\lambda^{-1}(x))}, J_\lambda(x) = |\det \nabla_x T_\lambda(x)|. \quad (2)$$

In this case the optimization in Eq. (1) can be rewritten using a transformation of variables as

$$\lambda^* = \arg \min_{\lambda \in \Lambda} \int q_0(x) \log \frac{q_0(x)}{J_\lambda(x)p(T_\lambda(x))} dx. \quad (3)$$

One can solve the optimization problem Eq. (3) using unbiased stochastic estimates of the gradient¹ with respect to

¹We assume throughout that differentiation and integration can be swapped wherever necessary.

λ based on draws from q_0 (Salimans and Knowles, 2013; Kingma and Welling, 2014),

$$\nabla_{\lambda} D_{\text{KL}}(q_{\lambda} || \pi) \approx \nabla_{\lambda} \log \frac{q_0(X)}{J_{\lambda}(X)p(T_{\lambda}(X))}, X \sim q_0.$$

2.2 Measure-preserving and ergodic maps

Variational flows are often constructed from a flexible, general-purpose parametrized family $\{T_{\lambda} : \lambda \in \Lambda\}$ that is not specialized for any particular target distribution (Papamakarios et al., 2021); it is the job of the KL divergence minimization Eq. (3) to adapt the parameter λ such that q_{λ} becomes a good approximation of the target π . However, there are certain functions—in particular, those that are both *measure-preserving* and *ergodic* for π —that naturally provide a means to approximate expectations of interest under π without the need for tuning. Intuitively, a measure-preserving map T will not change the distribution of draws from π : if $X \sim \pi$, then $T(X) \sim \pi$. And an ergodic map T , when applied repeatedly, will not get “stuck” in a subset of \mathcal{X} unless it has probability either 0 or 1 under π . The precise definitions are given in Definitions 2.1 and 2.2.

Definition 2.1 (Measure-preserving map (Eisner et al., 2015, pp. 73, 105)). A measurable function $T : \mathcal{X} \rightarrow \mathcal{X}$ is measure-preserving for π if $T\pi = \pi$, where $T\pi$ is the push-forward measure given by $\pi(T^{-1}(A))$ for each measurable set $A \subseteq \mathcal{X}$.

Definition 2.2 (Ergodic map (Eisner et al., 2015, pp. 73, 105)). A measurable function $T : \mathcal{X} \rightarrow \mathcal{X}$ is ergodic for π if for all measurable sets $A \subseteq \mathcal{X}$, $T(A) = A$ implies that $\pi(A) \in \{0, 1\}$.

If a map T satisfies both Definitions 2.1 and 2.2, then long-run averages resulting from repeated applications of T will converge to expectations under π , as shown by Theorem 2.3. When \mathcal{X} is compact, this result shows that the discrete measure $\frac{1}{N} \sum_{n=0}^{N-1} \delta_{T^n x}$ converges weakly to π (Dajani and Dirksin, 2008, Theorem 6.1.7).

Theorem 2.3 (Ergodic Theorem [Birkhoff, 1931; Eisner et al., 2015, p. 212]). Suppose $T : \mathcal{X} \rightarrow \mathcal{X}$ is measure-preserving and ergodic for π , and $f \in L^1(\pi)$. Then

$$\lim_{N \rightarrow \infty} \frac{1}{N} \sum_{n=0}^{N-1} f(T^n x) = \int f d\pi \quad \pi\text{-a.e. } x \in \mathcal{X}.$$

Fig. 1a provides an example illustration of this result when π is the uniform distribution $\text{Unif}[0, 1]$, $T : [0, 1] \rightarrow [0, 1]$ is the shift map $T(x) = x + \lambda \pmod{1}$ for some $\lambda \in \mathbb{R}$, and x is initialized at 0.5. In particular, for any irrational $\lambda \in \mathbb{R}$ (here $\pi/16$), the shift map is both measure-preserving and ergodic for π . As the number of applications increases, the collection of iterates $(T^n x)_{n=0}^N$ forms a discrete approximation to $\text{Unif}[0, 1]$. On the other hand, for a rational $\lambda \in \mathbb{R}$

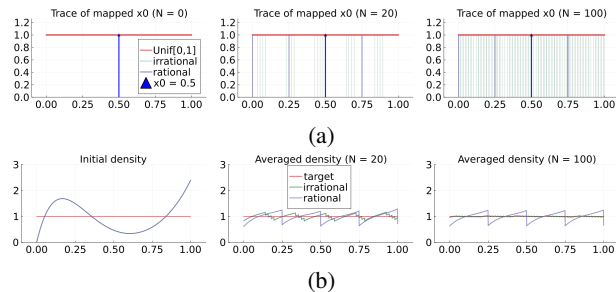


Figure 1: The effect of the shift map $T(x) = x + \lambda \pmod{1}$ for shift $\lambda \in \mathbb{R}$. Note that T is measure-preserving for $\pi = \text{Unif}[0, 1]$. Green denotes irrational $\lambda = \pi/16$, blue denotes rational $\lambda = 1/4$, and the red line shows the uniform density. (1a): Starting from $x = 0.5$, repeated application of an irrational shift map eventually creates a discrete probability measure that converges weakly to $\text{Unif}[0, 1]$; the rational shift map is periodic and so does not exhibit this behaviour. (1b): Starting from a mixture of beta distributions, averaging over repeated applications of the shift map does converge to $\text{Unif}[0, 1]$ in total variation when λ is irrational.

(here $1/4$), the shift map is measure-preserving but not ergodic. In this case the iterates are trapped in the finite set $\{0, 0.25, 0.5, 0.75, 1\}$ and do not approximate $\text{Unif}[0, 1]$.

3 Ergodic variational flows

In this section, we develop a parametrized family of *ergodic variational flows* that enable tractable i.i.d. sampling and density evaluation, and that converge to the target distribution both weakly and in total variation in the limit of increasingly many flow steps (Theorems 3.1 and 3.2) regardless of parameter tuning effort. Thus, ergodic variational flows provide the same compelling convergence result as MCMC, but with the added benefit of i.i.d. sampling and density evaluation, and hence unbiased ELBO estimates.

3.1 Variational family

Define a reference distribution q_0 on \mathcal{X} for which i.i.d. sampling and density evaluation is tractable, and a collection of measurable functions $T_{\lambda} : \mathcal{X} \rightarrow \mathcal{X}$ parametrized by $\lambda \in \Lambda$ such that for each parameter value λ , the map T_{λ} is measure-preserving and ergodic for π . Then the *ergodic variational flow family* generated by q_0 and T_{λ} is the collection of distributions

$$q_{\lambda, N} = \frac{1}{N} \sum_{n=0}^{N-1} T_{\lambda}^n q_0 \quad \text{for } \lambda \in \Lambda, N \in \mathbb{N},$$

where $T_{\lambda}^n q_0$ denotes the pushforward of the distribution q_0 under n repeated applications of T_{λ} . Fig. 1b displays a simple example of this family where q_0 is a mixture of beta distributions $q_0 = 0.6 \cdot \text{Beta}(2, 6) + 0.4 \cdot \text{Beta}(6, 1)$

and T_λ is the shift map $T_\lambda(x) = x + \lambda \bmod 1$ for $\lambda = \pi/16$. Because T_λ is measure-preserving and ergodic for $\text{Unif}[0, 1]$, the uniformly-weighted average of $T_\lambda^n q_0$ from $n = 0, \dots, N$ converges in total variation to $\text{Unif}[0, 1]$. In fact, any irrational λ will provide the same result (although the speed of convergence of $q_{\lambda, N}$ to $\text{Unif}[0, 1]$ will depend on λ). Thus the proposed ergodic variational flow family $\{q_{\lambda, N} : \lambda \in \Lambda, N \in \mathbb{N}\}$ achieves the same ‘‘convergence regardless of tuning’’ enjoyed by MCMC methods. Section 3.2 shows that this result extends generally.

3.2 Convergence guarantees

In this section, we show that for all $\lambda \in \Lambda$, the distribution $q_{\lambda, N}$ converges to π as $N \rightarrow \infty$ (proofs may be found in Appendix A). Thus, regardless of the ability to tune the parameter λ , we are guaranteed that $q_{\lambda, N}$ can arbitrarily approximate π given enough computational effort (i.e., large enough N). In particular, we demonstrate this convergence in three senses: weak, setwise, and in total variation. Recall that a sequence of probability distributions q_n converges *weakly* to π if for all bounded, continuous $f : \mathcal{X} \rightarrow \mathbb{R}$, $\lim_{n \rightarrow \infty} \int f(x) q_n(dx) = \int f(x) \pi(dx)$, and converges *setwise* to π if for all measurable $A \subseteq \mathcal{X}$, $\lim_{n \rightarrow \infty} q_n(A) = \pi(A)$.

Theorem 3.1. *Suppose $q_0 \ll \pi$ and T_λ is measure-preserving and ergodic for π . Then $q_{\lambda, N}$ converges both setwise and weakly to π as $N \rightarrow \infty$.*

We obtain a stronger result—convergence in total variation—when we can express the density of $q_{\lambda, N}$ using the transformation of variables formula Eq. (2). Recall that a sequence of distributions q_n converges in *total variation* to π if $D_{\text{TV}}(q_n, \pi) = \sup_A |q_n(A) - \pi(A)| \rightarrow 0$ as $n \rightarrow \infty$.

Theorem 3.2. *Suppose $q_0 \ll \pi$, T_λ is a diffeomorphism, and T_λ is measure-preserving and ergodic for π . Then $q_{\lambda, N}$ converges in total variation to π as $N \rightarrow \infty$.*

This result is asymptotic in nature, which suffices for our purposes to guarantee that the family can well-approximate the target π in the large- N limit; in practice we use the ELBO (see Section 3.4) to tune λ and N . Although similar nonasymptotic results exist for the ergodic average law of Markov chains (Roberts and Rosenthal, 1997), the required technical conditions (minorization and drift conditions) do not apply to our deterministic setting. It is also worth noting that while Theorem 3.2 pertains to the total variation distance, the KL divergence is more relevant in the context of variational inference. However, a small total variation distance implies a small KL divergence in many practical scenarios, e.g., when the density ratio $q(x)/\pi(x)$ is bounded (Proposition A.3 (Verdú, 2014, Theorem 7)).

Algorithm 1 $\text{Sample}(q_{\lambda, N})$: Take a draw from $q_{\lambda, N}$

Require: reference distribution q_0 , flow map T_λ , number of steps N
 $K \leftarrow \text{Sample}(\text{Unif}\{0, 1, \dots, N-1\})$
 $x_0 \leftarrow \text{Sample}(q_0)$
return $T_\lambda^K(x_0)$

Algorithm 2 $\log q_{\lambda, N}(x)$: Evaluate the log-density of $q_{\lambda, N}$

Require: location x , reference distribution q_0 , flow map T_λ , Jacobian J_λ , number of steps N
 $L \leftarrow 0$
 $w_0 \leftarrow \log q_0(x)$
for $n = 1, \dots, N-1$ **do**
 $x \leftarrow T_\lambda^{-1}(x)$
 $L \leftarrow L + \log J_\lambda(x)$
 $w_n \leftarrow \log q_0(x) - L$
end for
return $\text{LogSumExp}(w_0, \dots, w_{N-1}) - \log N$

Algorithm 3 $\text{EstELBO}(\lambda, N)$: Obtain an unbiased estimate of the ELBO for $q_{\lambda, N}$.

Require: reference q_0 , unnormalized target p , flow map T_λ , Jacobian J_λ , number of flow steps N
 $x_0 \leftarrow \text{Sample}(q_0)$, $J_0 \leftarrow J_\lambda(x_0)$
for $n = 1, \dots, N-1$ **do**
 $x_n \leftarrow T_\lambda(x_{n-1})$, $J_n \leftarrow J_\lambda(x_n)$
 $x_{-n} \leftarrow T_\lambda^{-1}(x_{-n+1})$, $J_{-n} \leftarrow J_\lambda(x_{-n})$
end for
 $z_0 \leftarrow q_{\lambda, N}(x_0)$ (via Algorithm 2)
 $J \leftarrow \prod_{j=1}^{N-1} J_{-j}$
for $n = 1, \dots, N-1$ **do**
 $\bar{q}_n \leftarrow \frac{1}{N} q_0(x_{-N+n}) / J$
 $z_n \leftarrow (z_{n-1} - \bar{q}_n) / J_{n-1} + \frac{1}{N} q_0(x_n)$
if $n < N-1$ **then**
 $J \leftarrow J \cdot J_{n-1} / J_{-N+n}$
end if
end for
 $\widehat{\text{ELBO}}(\lambda, N) \leftarrow \frac{1}{N} \sum_{n=0}^{N-1} (\log p(x_n) - \log z_n)$
return $\widehat{\text{ELBO}}(\lambda, N)$

3.3 Density evaluation and sampling

If $T_\lambda : \mathcal{X} \rightarrow \mathcal{X}$ is a diffeomorphism with Jacobian $J_\lambda : \mathcal{X} \rightarrow \mathbb{R}$, we can express the density of $q_{\lambda, N}$ by using a transformation of variables formula on each component in the mixture:

$$q_{\lambda, N}(x) = \frac{1}{N} \sum_{n=0}^{N-1} \frac{q_0(T_\lambda^{-n}x)}{\prod_{j=1}^n J_\lambda(T_\lambda^{-j}x)}.$$

This density can be computed efficiently using $N-1$ evaluations of T_λ^{-1} and J_λ each (Algorithm 2). For sampling, we can obtain an independent draw $X \sim q_{\lambda, N}$ by treating

$q_{\lambda,N}$ as a mixture of N distributions:

$$K \sim \text{Unif}\{0, 1, \dots, N-1\} \quad X_0 \sim q_0 \quad X = T_\lambda^K(X_0).$$

The procedure is given in Algorithm 1. On average, this computation requires $\mathbb{E}[K] = \frac{N-1}{2}$ applications of T_λ , and at most it requires $N-1$ applications.

However, in practice, one often takes samples from $q_{\lambda,N}$ to estimate the expectation of some test function $f : \mathcal{X} \rightarrow \mathbb{R}$. In this case, one can use all intermediate states over a single pass of a trajectory rather than use individual i.i.d. samples. In particular, we obtain an unbiased estimate of $\int f(x)q_{\lambda,N}(dx)$ via

$$X_0 \sim q_0 \quad \frac{1}{N} \sum_{n=0}^{N-1} f(T_\lambda^n X_0).$$

We refer to this estimate as the *trajectory-averaged estimate* of f . The trajectory-averaged estimate of f is preferred over the naïve estimate based on a single draw $f(X)$, $X \sim q_{\lambda,N}$, as its cost is of the same order ($N-1$ applications of T_λ) but it typically has a significantly lower variance; see Proposition A.1.

3.4 ELBO estimation

We can minimize the KL divergence from $q_{\lambda,N}$ to π by maximizing the ELBO (Blei et al., 2017), given by

$$\begin{aligned} \text{ELBO}(\lambda, N) &= \int q_{\lambda,N}(x) \log \frac{p(x)}{q_{\lambda,N}(x)} dx \\ &= \int q_0(x) \left(\frac{1}{N} \sum_{n=0}^{N-1} \log \frac{p(T_\lambda^n x)}{q_{\lambda,N}(T_\lambda^n x)} \right) dx. \end{aligned}$$

The trajectory-averaged ELBO estimate is thus

$$X_0 \sim q_0, \quad \widehat{\text{ELBO}}(\lambda, N) = \frac{1}{N} \sum_{n=0}^{N-1} \log \frac{p(T_\lambda^n X_0)}{q_{\lambda,N}(T_\lambda^n X_0)}. \quad (4)$$

The naïve method to compute this estimate—sampling X_0 and then computing the log density ratio for each term—requires $O(N^2)$ computation because each evaluation of $q_{\lambda,N}(x)$ is $O(N)$. Algorithm 3 provides an efficient way of computing $\widehat{\text{ELBO}}(\lambda, N)$ in $O(N)$ operations, which is on par with taking a single draw from $q_{\lambda,N}$ or evaluating $q_{\lambda,N}(x)$ once. The key insight in Algorithm 3 is that we can evaluate the collection of values $\{q_{\lambda,N}(X_0), q_{\lambda,N}(T_\lambda X_0), \dots, q_{\lambda,N}(T_\lambda^{N-1} X_0)\}$ incrementally, starting from $q_{\lambda,N}(X_0)$ and iteratively computing each $q_{\lambda,N}(T_\lambda^n X_0)$ for increasing n in constant time. Note that Algorithm 3 still requires $O(N)$ memory; Algorithm 5 in Appendix B provides an $O(N)$ time, $O(1)$ memory implementation of Eq. (4).

3.5 Numerical stability

Density evaluation (Algorithm 2) and ELBO estimation (Algorithm 3) both involve repeated applications of T_λ and T_λ^{-1} . This poses no issue in theory, but in a computer—where floating point computations are used—it is critical to code the map T_λ and its inverse T_λ^{-1} in a numerically precise way such that the composition of $(T_\lambda^K) \circ (T_\lambda^{-K})$ is the identity map for large $K \in \mathbb{N}$. In practice, we check the limits of stability of our flow implementation by taking draws from q_0 and evaluating T_λ^K followed by T_λ^{-K} (and vice versa) for increasing K until we cannot reliably invert the flow. See Fig. 7 in the appendix for an example usage of this diagnostic. Note that for sample generation specifically (Algorithm 1), numerical stability is not a concern as it only requires forward evaluation of the map T_λ .

4 Hamiltonian ergodic variational flows

In this section, we provide an implementation of an ergodic variational flow based on Hamiltonian dynamics. The construction is inspired by Hamiltonian Monte Carlo (HMC) (Neal, 2011, 1996), in which each iteration involves simulating Hamiltonian dynamics followed by a stochastic momentum refreshment; our method replaces the stochastic refreshment with a deterministic transformation. In particular, consider the *augmented* target density on $\mathcal{X} \times \mathbb{R}^d \times [0, 1]$,

$$\bar{\pi}(x, \rho, u) = \pi(x) m(\rho) \mathbb{1}[0 \leq u \leq 1], \quad m(\rho) = \prod_{i=1}^d r(\rho_i),$$

with auxiliary variables $\rho \in \mathbb{R}^d$, $u \in [0, 1]$, and some almost-everywhere differentiable univariate probability density $r : \mathbb{R} \rightarrow \mathbb{R}_+$. The x -marginal distribution of $\bar{\pi}$ is the original target distribution π ; therefore if we are able to obtain i.i.d. draws from $\bar{\pi}$, we can obtain i.i.d. draws from π by simply discarding the ρ and u components. We construct T_λ by composing the following three steps in sequence:

(1) Hamiltonian dynamics We first apply

$$(x', \rho') \leftarrow H_L(x, \rho),$$

where $H_L : \mathcal{X} \times \mathbb{R}^d \rightarrow \mathcal{X} \times \mathbb{R}^d$ is the map of Hamiltonian dynamics with position x and momentum ρ simulated for a time interval of length $L \in \mathbb{R}_+$,

$$\frac{d\rho}{dt} = \nabla \log \pi(x) \quad \frac{dx}{dt} = -\nabla \log m(\rho). \quad (5)$$

One can show that this preserves density (and hence is measure preserving) and it is also unit Jacobian (Neal, 2011).

(2) Pseudotime shift Second, we apply a constant shift to the pseudotime variable u ,

$$u' \leftarrow u + \xi \pmod{1},$$

where $\xi \in \mathbb{R}$ is a fixed irrational number (say, $\xi = \pi/16$). As this is a constant shift, it is unit Jacobian and density-preserving (and hence measure-preserving). The u component will act as a notion of “time” of the flow, and ensures that the refreshment of ρ in step (3) below will take a different form even if x visits the same location again.

(3) Momentum refreshment Finally, we refresh the momentum variables via

$$\forall i = 1, \dots, d, \quad \rho_i'' \leftarrow R^{-1}(R(\rho_i') + z(x_i', u') \pmod{1}),$$

where R is the cumulative distribution function (CDF) of density r , and $z : \mathcal{X} \times [0, 1] \rightarrow \mathbb{R}$ is a differentiable “pseudorandom” function, e.g., $z(x_i, u) = \sin(ax_i + u)$ for some large value of $a \in \mathbb{R}$; this generalizes the map from Neal (2012); Murray and Elliott (2012) to enable the shift to depend on the state x and pseudotime u . In essence, this step (3) is an attempt to replicate the independent resampling of $\rho \sim m$ from HMC using only deterministic maps. This map is measure-preserving as it involves mapping the momentum to a $\text{Unif}[0, 1]$ random variable via the CDF, shifting by an amount that only depends on x, u , and then mapping back using the inverse CDF. The Jacobian is the joint momentum density ratio $m(\rho')/m(\rho'')$.

Composition of (1-3) The composition of these three steps forms a measure-preserving map T_λ for the augmented target $\bar{\pi}$. Note that the variational parameter λ can include any parameter in these steps that maintains the measure-preserving nature of T_λ . For example, $\lambda = (L, \xi)$, where $L \in \mathbb{R}_+$ is the simulation length in step 1 and $\xi \in \mathbb{R}$ is the shift parameter in step 2.

Practical implementation In practice, we cannot simulate the dynamics in step (1) perfectly. Instead, we approximate the dynamics in Eq. (5) by running L steps of the leapfrog method, where each leapfrog map $\hat{H}_\epsilon : \mathbb{R}^{2d} \rightarrow \mathbb{R}^{2d}$ involves interleaving three discrete transformations with step size $\epsilon > 0$,

$$\begin{aligned} \hat{\rho}_{k+1} &= \rho_k + \frac{\epsilon}{2} \nabla \log \pi(x_k) \\ x_{k+1} &= x_k - \epsilon \nabla \log m(\hat{\rho}_{k+1}) \\ \rho_{k+1} &= \hat{\rho}_{k+1} + \frac{\epsilon}{2} \nabla \log \pi(x_{k+1}) \end{aligned}$$

Denote the map $T_{\lambda, \epsilon}$ to be the composition of the three steps with Hamiltonian dynamics replaced by the leapfrog integrator; Algorithm 6 provides the pseudocode in Appendix C. Note that this map does not maintain invariance of $\bar{\pi}$ due to the discretized steps. To address this, we could make $T_{\lambda, \epsilon}$ arbitrarily close to measure-preserving by making ϵ quite small; but rather than that, we can simply *tune* ϵ as a variational parameter in addition to λ by maximizing the ELBO. Indeed, in our experiments, we find that the optimal

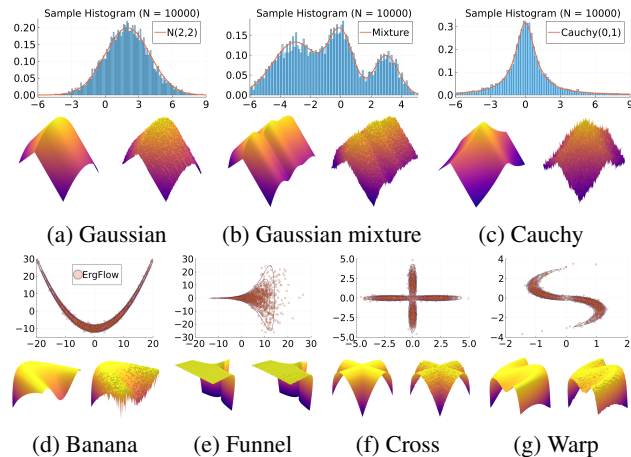


Figure 2: Marginal sample histograms (first row) and pairs of exact and approximate joint log density (second row) for Gaussian (2a), mixture (2b), and Cauchy (2c) targets. Marginal sample scatter (third row), pairs of sliced exact and approximate joint log density (fourth row) for banana (2d), funnel (2e), cross (2f), and warped Gaussian (2g) targets.

step size ϵ is not vanishingly small, but instead trades off simulation fidelity and computational efficiency.

In our experiments we tune the number of leapfrog steps $\lambda = L$ and the step size ϵ by maximizing the ELBO. We also tune the number of refreshments N to achieve a desirable computation-quality tradeoff by visually inspecting the convergence of the ELBO.

5 Experiments

In this section, we demonstrate the performance of our method (`ErgFlow`) on 7 synthetic and 7 real data targets, which include a range of challenging features such as heavy tails, high dimensions, multimodality, and weak identifiability. We compare the posterior approximation quality against several black-box normalizing flow methods (NF): `PlanarFlow`, `RadialFlow`, and `RealNVP` with various architectural settings (Papamakarios et al., 2021). To make the methods comparable via the ELBO, we train all NFs on the same joint space as `ErgFlow`. We also compare the marginal sample quality of `ErgFlow` against 5,000 samples from NUTS and NFs. Finally, we compare sampling time with all competitors, and effective sample size (ESS) per second with HMC. For all experiments, we use the standard Laplace distribution as the momentum distribution; although Gaussians are more commonly used in HMC, we find that the Laplace was more numerically stable to work with (see Fig. 7 in Appendix E). More experimental details may be found in Appendix E. All experiments were conducted on a machine with an AMD Ryzen 9 3900X and 32GB of RAM.

5.1 Qualitative assessment

We begin with a qualitative examination of the i.i.d. samples and the approximated targets produced by `ErgFlow` initialized at $q_0 = \mathcal{N}(0, 1)$ for three one-dimensional synthetic distributions: a Gaussian, a mixture of Gaussians, and the standard Cauchy. We excluded the pseudotime variable u here in order to visualize the full joint density of (x, ρ) in 2 dimensions. More details can be found in Appendix E.1. Figs. 2a to 2c show histograms of 10,000 i.i.d. x -marginal samples generated by `ErgFlow` for each of the three targets, all of which nearly perfectly match the true target marginals. Figs. 2a to 2c also show that $\log q_{\lambda, N}$ is generally a good approximation of the log joint target density.

We then present similar visualizations on four more challenging synthetic target distributions: the banana (Haario et al., 2001), Neal’s funnel (Neal, 2003), a cross-shaped Gaussian mixture, and a warped Gaussian. All four examples have a 2-dimensional state $x \in \mathbb{R}^2$, and hence $(x, \rho, u) \in \mathbb{R}^5$. In each example we set the initial distribution q_0 to be the mean-field Gaussian approximation. More details can be found in Appendix E.2. Figs. 2d to 2g shows the scatter plots consisting of 1,000 i.i.d. x -marginal samples drawn from `ErgFlow`, as well as the approximated `ErgFlow` log density and exact log density sliced as a function of $x \in \mathbb{R}^2$ for a single value of (ρ, u) chosen randomly via $(\rho, u) \sim \text{Lap}(0, I) \times \text{Unif}[0, 1]$ (which is required for visualization, as $(x, \rho, u) \in \mathbb{R}^5$). We see that, qualitatively, both the samples and approximated densities from `ErgFlow` closely match the target. Finally, Fig. 8 in Appendix E.2 provides a more comprehensive set of sample histograms (showing the x -, ρ -, and u -marginals). These visualizations confirm our theory that `ErgFlow` exhibits MCMC-like convergence.

5.2 Posterior approximation quality

Next, we provide a quantitative comparison of `ErgFlow`, NFs, and NUTS on 7 real data experiments outlined in Appendix E.4. We tune each NF method under various settings (Tables 1 and 2 and Appendix E.4.5), and present the best one for each example. ELBOs of `ErgFlow` are estimated with Algorithm 3, averaging over 1,000 independent trajectories. ELBOs of NFs are based on 2,000 samples. To obtain an assessment for the target marginal distribution itself (not the augmented target), we also compare methods using the kernel Stein discrepancy (KSD) with an inverse quadratic (IMQ) kernel (Gorham and Mackey, 2017). Both NUTS and NFs use 5,000 samples for KSD estimation, while `ErgFlow` is based on 2,000 i.i.d. draws (Algorithm 1). For KSD comparisons, all variational methods are tuned by maximizing the ELBO (Figs. 3 and 14).

Augmented target distribution Fig. 3 displays the ELBO comparison. First, Fig. 3a shows how different step

sizes ϵ and number of refreshments N affects approximation quality. Overly large step sizes typically result in errors due to the use of discretized Hamiltonian dynamics, while overly small step sizes result in a flow that makes slow progress towards the target. `ErgFlow` with a tuned step size generally shows a comparable joint ELBO value to the best NF method, yielding a competitive target approximation. Similar comparisons and assessment of the effect of step size for the synthetic examples are presented in Figs. 6, 9 and 13. Note that in three examples (Figs. 3a, 3d and 3g), the tuned `RealNVP` ELBO exceeds `ErgFlow` by a small amount; but this required expensive architecture search and parameter tuning, and as we will describe next, `ErgFlow` is actually more reliable in terms of target marginal sample quality and density estimation.

Original target distribution The second row of Fig. 3 displays a comparison of KSD for the target distribution itself (instead of the augmented target). In particular, `ErgFlow` produces comparable sample quality to that from NUTS—an exact MCMC method—and clearly outperforms all of the NF competitors. The scatter plots of samples in Fig. 16 confirm the improvement in sample quality of `ErgFlow` over variational competitors. Further, Fig. 4 shows the (sliced) densities on two difficult real data examples: Bayesian student-t regression (with a heavy-tailed posterior), and a high-dimensional sparse regression (parameter dimension is 84). This result demonstrates that the densities provided by `ErgFlow` more closely match those of the original target distribution than those of the best NF. Notice that `ErgFlow` accurately captures the skew and heavy tails of the exact target, while the NF density fails to do so and contains many spurious modes.

5.3 Ease of tuning

In order to tune `ErgFlow`, we simply run a 1-dimensional parameter sweep for the step size ϵ , and use a visual inspection of the ELBO to set an appropriate number of flow steps N . In contrast, tuning an NF requires optimizing its architecture, number of layers, and its (typically many) parameters. Not only is this time consuming—in our experiments, tuning took 10 minutes to roughly 1 hour (Fig. 5)—but the optimization can also behave in unintuitive ways. For example, performance can be heavily dependent on the number of flow layers, and adding more layers does not necessarily improve quality. Fig. 13, Tables 1 and 2, and Appendix E.4.5 show that using more layers does not necessarily help, and slows tuning considerably. In the case of `RealNVP` specifically, tuning can be unstable, especially for more complex models. The optimizer often returns NaN values for flow parameters during training (see Table 1). This instability has been noted in earlier work (Dinh et al., 2017, Sec. 3.7).

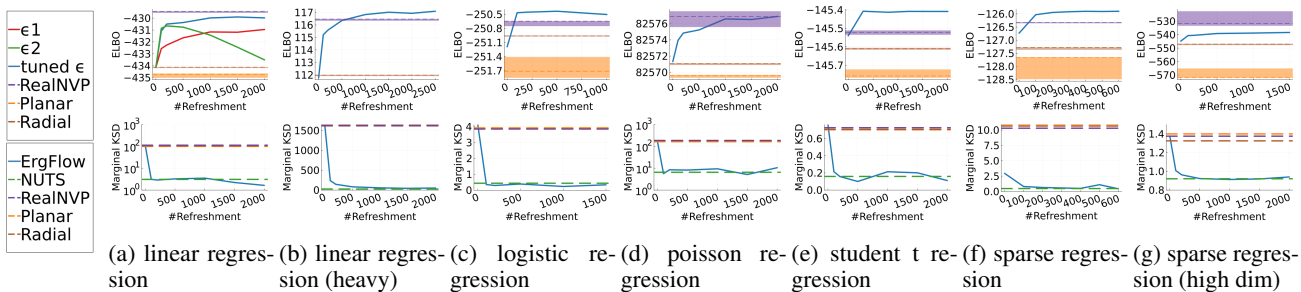


Figure 3: ELBO and KSD comparison for real data examples. Fig. 3a displays the effect of step size for the linear regression problem: $\epsilon_1 = 0.0001$, $\epsilon_2 = 0.001$ and tuned $\epsilon = 0.0005$; see Fig. 14 for step sizes for all other experiments. Lines indicate the median, and error regions indicate 25th to 75th percentile from 5 runs. Fig. 3b does not include ELBOs of PlanarFlow as values are significantly worse than all other methods and are hard to visualize (see its ELBOs in Fig. 14a).

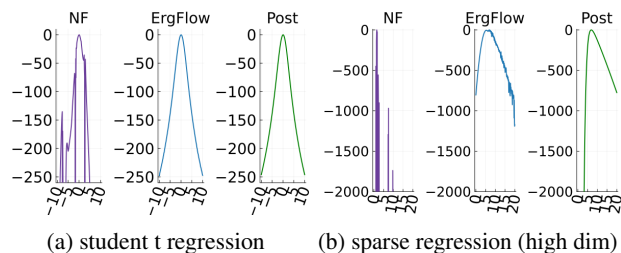


Figure 4: Sliced log conditional densities on student-t regression (Fig. 4a) and high-dimensional sparse regression (Fig. 4b). We visualize the log conditional density of the first coordinate by fixing other coordinates to value 0. The NF methods are chosen to be the best performing ones from Figs. 3e and 3g. Since we only know the log posterior density up to an unknown normalizing constant, we shift all log densities to have maximal value 0 for visualization.

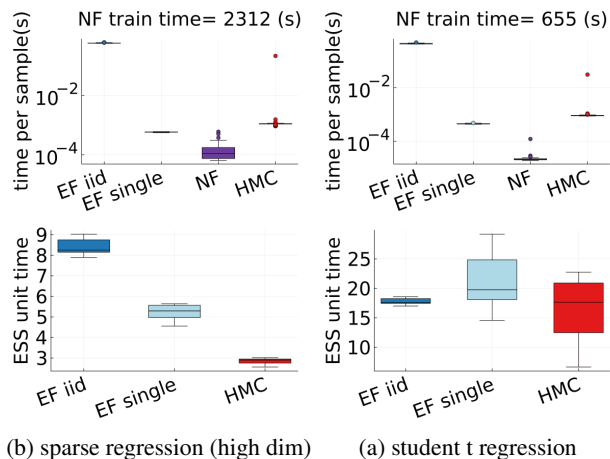


Figure 5: Timing results (100 trials), showing sampling time (first row) and ESS per second (second row).

5.4 Time efficiency

Finally, Fig. 5 presents timing results for two of the real data experiments (additional comparisons in Figs. 11 and 15).

In this figure, we use EF_{iid} to refer to i.i.d. sampling from ErgFlow, and EF_{single} to refer to collecting all intermediate states on a single trajectory. This result shows that the per sample time of EF_{single} is similar to NUTS and HMC, as one would expect. EF_{iid} is the slowest because each sample is generated by passing through the entire flow. The NF generates the fastest draws, but recall that this comes at the cost of significant initial tuning time; in the time it takes NF to generate its first sample, $ErgFlow_{single}$ has generated millions of samples in Fig. 5. See Appendix E.3.1 for a detailed discussion of this trade-off.

Figs. 5 and 15 further show the computational efficiency in terms of ESS per second on real data examples, which reflects the autocorrelation between drawn samples. In practice, a dependent sample sequence with lower ESS usually has a lower estimation power. Results show that $ErgFlow$ produce comparable ESS per second to HMC. EF_{single} behaves similarly to HMC as expected since the pseudo-momentum refreshment we proposed (steps (2-3) of Section 4) resembles the momentum resample step of HMC. The ESS efficiency of EF_{iid} depends on the trade-off between a slower sampling time and i.i.d. nature of drawn samples. In these real data examples, EF_{iid} typically produces a high ESS per second; but in the synthetic examples (Fig. 11b), EF_{iid} is similar to the others.

6 Conclusion

This work presented ergodic variational flows, a new variational family that provides tractable i.i.d. sampling, density evaluation, and MCMC-like convergence guarantees. Experiments demonstrate a comparable sample quality to NUTS and more reliable posterior approximations than standard normalizing flows. A main limitation of our methodology is numerical stability; reversing the flow for long trajectories can be unstable in practice. Future work includes developing more stable momentum refreshment schemes and extensions via involutive MCMC (Neklyudov et al., 2020; Spanbauer et al., 2020; Neklyudov and Welling, 2022).

References

- Christian Robert and George Casella. *Monte Carlo Statistical Methods*. Springer, 2nd edition, 2004.
- Christian Robert and George Casella. A short history of Markov Chain Monte Carlo: subjective recollections from incomplete data. *Statistical Science*, 26(1):102–115, 2011.
- Andrew Gelman, John Carlin, Hal Stern, David Dunson, Aki Vehtari, and Donald Rubin. *Bayesian data analysis*. CRC Press, 3rd edition, 2013.
- Gareth Roberts and Jeffrey Rosenthal. General state space Markov chains and MCMC algorithms. *Probability Surveys*, 1:20–71, 2004.
- Jackson Gorham and Lester Mackey. Measuring sample quality with Stein’s method. In *Advances in Neural Information Processing Systems*, 2015.
- Qiang Liu, Jason Lee, and Michael Jordan. A kernelized Stein discrepancy for goodness-of-fit tests and model evaluation. In *International Conference on Machine Learning*, 2016.
- Kacper Chwialkowski, Heiko Strathmann, and Arthur Gretton. A kernel test of goodness of fit. In *International Conference on Machine Learning*, 2016.
- Jackson Gorham and Lester Mackey. Measuring sample quality with kernels. In *International Conference on Machine Learning*, 2017.
- Andreas Anastasiou, Alessandro Barp, François-Xavier Briol, Bruno Ebner, Robert Gaunt, Fatemeh Ghaderinezhad, Jackson Gorham, Arthur Gretton, Christophe Ley, Qiang Liu, Lester Mackey, Chris Oates, Gesine Reinert, and Yvik Swan. Stein’s method meets statistics: a review of some recent developments. *arXiv:2105.03481*, 2021.
- Li Wenliang and Heishiro Kanagawa. Blindness of score-based methods to isolated components and mixing proportions. *arXiv:2008.10087*, 2020.
- Jonathan Huggins and Lester Mackey. Random feature Stein discrepancies. In *Advances in Neural Information Processing Systems*, 2018.
- Wenbo Gong, Yingzhen Li, and José Miguel Hernández-Lobato. Sliced kernelized Stein discrepancy. In *International Conference on Learning Representations*, 2021.
- Andrew Gelman and Donald Rubin. Inference from iterative simulation using multiple sequences. *Statistical Science*, 7(4):457–472, 1992.
- Stephen Brooks and Andrew Gelman. General methods for monitoring convergence of iterative simulations. *Journal of Computational and Graphical Statistics*, 7(4):434–455, 1998.
- John Geweke. Evaluating the accuracy of sampling-based approaches to the calculation of posterior moments. In J. M. Bernardo, J. O. Berger, and A. P. Dawid, editors, *Bayesian Statistics*, volume 4, pages 169–193, 1992.
- Mary Kathryn Cowles and Bradley Carlin. Markov chain Monte Carlo convergence diagnostics: a comparative review. *Journal of the American Statistical Association*, 91(434):883–904, 1996.
- Michael Jordan, Zoubin Ghahramani, Tommi Jaakkola, and Lawrence Saul. An introduction to variational methods for graphical models. *Machine Learning*, 37:183–233, 1999.
- Martin Wainwright and Michael Jordan. Graphical models, exponential families, and variational inference. *Foundations and Trends in Machine Learning*, 1(1–2):1–305, 2008.
- David Blei, Alp Kucukelbir, and Jon McAuliffe. Variational inference: a review for statisticians. *Journal of the American Statistical Association*, 112(518):859–877, 2017.
- Danilo Rezende and Shakir Mohamed. Variational inference with normalizing flows. In *International Conference on Machine Learning*, 2015a.
- Rajesh Ranganath, Dustin Tran, and David Blei. Hierarchical variational models. In *International Conference on Machine Learning*, 2016.
- George Papamakarios, Eric Nalisnick, Danilo Jimenez Rezende, Shakir Mohamed, and Balaji Lakshminarayanan. Normalizing flows for probabilistic modeling and inference. *Journal of Machine Learning Research*, 22:1–64, 2021.
- Solomon Kullback and Richard Leibler. On information and sufficiency. *The Annals of Mathematical Statistics*, 22(1):79–86, 1951.
- Matthew D. Hoffman, David M. Blei, Chong Wang, and John Paisley. Stochastic variational inference. *Journal of Machine Learning Research*, 14:1303–1347, 2013.
- Rajesh Ranganath, Sean Gerrish, and David Blei. Black box variational inference. In *International Conference on Artificial Intelligence and Statistics*, 2014.
- Tommi Jaakkola and Michael Jordan. Improving the mean field approximation via the use of mixture distributions. In *Learning in graphical models*, pages 163–173. Springer, 1998.
- Samuel Gershman, Matthew Hoffman, and David Blei. Nonparametric variational inference. In *International Conference on Machine Learning*, 2012.
- O. Zoby. Variational Bayesian inference with Gaussian-mixture approximations. *Electronic Journal of Statistics*, 8:355–389, 2014.
- Fangjian Guo, Xiangyu Wang, Kai Fan, Tamara Broderick, and David Dunson. Boosting variational inference. In *Advances in Neural Information Processing Systems*, 2016.
- Xiangyu Wang. Boosting variational inference: theory and examples. Master’s thesis, Duke University, 2016.
- Andrew Miller, Nicholas Foti, and Ryan Adams. Variational boosting: iteratively refining posterior approximations. In *International Conference on Machine Learning*, 2017.
- Francesco Locatello, Rajiv Khanna, Joydeep Ghosh, and Gunnar Rätsch. Boosting variational inference: an optimization perspective. In *International Conference on Artificial Intelligence and Statistics*, 2018a.
- Francesco Locatello, Gideon Dresdner, Rajiv Khanna, Isabel Valera, and Gunnar Rätsch. Boosting black box variational inference. In *Advances in Neural Information Processing Systems*, 2018b.
- Trevor Campbell and Xinglong Li. Universal boosting variational inference. In *Advances in Neural Information Processing Systems*, 2019.
- Adrian Corduneanu and Christopher Bishop. Variational Bayesian model selection for mixture distributions. In *Artificial Intelligence and Statistics*, 2001.
- Sato Masa-aki. Online model selection based on the variational Bayes. *Neural Computation*, 13(7):1649–1681, 2001.
- Constantinos Constantinopoulos, Michalis Titsias, and Aristidis Likas. Bayesian feature and model selection for Gaussian mixture models. *IEEE Transactions on Pattern Analysis and Machine Intelligence*, 28(6):1013–1018, 2006.

- John Ormerod, Chong You, and Samuel Müller. A variational Bayes approach to variable selection. *Electronic Journal of Statistics*, 11(2):3549–3594, 2017.
- Badr-Eddine Chérif-Abdellatif and Pierre Alquier. Consistency of variational Bayes inference for estimation and model selection in mixtures. *Electronic Journal of Statistics*, 12(2):2995–3035, 2018.
- Chenyang Tao, Liqun Chen, Ruiyi Zhang, Ricardo Henao, and Lawrence Carin. Variational inference and model selection with generalized evidence bounds. In *International Conference on Machine Learning*, 2018.
- Zuheng Xu and Trevor Campbell. The computational asymptotics of variational inference and the Laplace approximation. *Statistics and Computing*, 32(4):1–37, 2022.
- Tim Salimans, Diederik Kingma, and Max Welling. Markov chain Monte Carlo and variational inference: bridging the gap. In *International Conference on Machine Learning*, 2015.
- Christopher Wolf, Maximilian Karl, and Patrick van der Smagt. Variational inference with Hamiltonian Monte Carlo. *arXiv:1609.08203*, 2016.
- Tomas Geffner and Justin Domke. MCMC variational inference via uncorrected Hamiltonian annealing. In *Advances in Neural Information Processing Systems*, 2021.
- Guodong Zhang, Kyle Hsu, Jianing Li, Chelsea Finn, and Roger Grosse. Differentiable annealed importance sampling and the perils of gradient noise. In *Advances in Neural Information Processing Systems*, 2021.
- Achille Thin, Nikita Kotelevskii, Alain Durmus, Maxim Panov, Eric Moulines, and Arnaud Doucet. Monte Carlo variational auto-encoders. In *International Conference on Machine Learning*, 2021a.
- Martin Jankowiak and Du Phan. Surrogate likelihoods for variational annealed importance sampling. *arXiv:2112.12194*, 2021.
- Radford Neal. Hamiltonian importance sampling. Banff International Research Station (BIRS) Workshop on Mathematical Issues in Molecular Dynamics, 2005.
- Anthony Caterini, Arnaud Doucet, and Dino Sejdinovic. Hamiltonian variational auto-encoder. In *Advances in Neural Information Processing Systems*, 2018.
- Naitong Chen, Zuheng Xu, and Trevor Campbell. Bayesian inference via sparse Hamiltonian flows. *arXiv:2203.05723*, 2022.
- Yichuan Zhang and José Miguel Hernández-Lobato. Ergodic inference: accelerate convergence by optimisation. In *International Conference on Learning Representations*, 2020.
- David Aldous and Hermann Thorisson. Shift-coupling. *Stochastic Processes and their Applications*, 44:1–14, 1993.
- Gareth Roberts and Jeffrey Rosenthal. Shift-coupling and convergence rates of ergodic averages. *Stochastic Models*, 13(1):147–165, 1997.
- Patrick Warren and Rosalind Allen. Trajectory reweighting for non-equilibrium steady states. *Molecular Physics*, 116(21–22):3104–3113, 2018.
- Grant Rotskoff and Eric Vanden-Eijnden. Dynamical computation of the density of states and Bayes factors using nonequilibrium importance sampling. *Physical Review Letters*, 122(15):150602, 2019.
- Greg Ver Steeg and Aram Galstyan. Hamiltonian dynamics with non-Newtonian momentum for rapid sampling. In *Advances in Neural Information Processing Systems*, 2021.
- Achille Thin, Yazid Janati, Sylvain Le Corff, Charles Ollion, Arnaud Doucet, Alain Durmus, Éric Moulines, and Christian Robert. NEO: non equilibrium sampling on the orbit of a deterministic transform. *arXiv:2103.10943*, 2021b.
- Kirill Neklyudov and Max Welling. Orbital MCMC. In *Artificial Intelligence and Statistics*, 2022.
- Matthew Hoffman and Andrew Gelman. The No-U-Turn Sampler: adaptively setting path lengths in Hamiltonian Monte Carlo. *Journal of Machine Learning Research*, 15(1):1593–1623, 2014.
- Radford Neal. MCMC using Hamiltonian dynamics. In Steve Brooks, Andrew Gelman, Galin Jones, and Xiao-Li Meng, editors, *Handbook of Markov chain Monte Carlo*, chapter 5. CRC Press, 2011.
- Danilo Rezende and Shakir Mohamed. Variational inference with normalizing flows. In *International Conference on Machine Learning*, pages 1530–1538. PMLR, 2015b.
- Laurent Dinh, Jascha Sohl-Dickstein, and Samy Bengio. Density estimation using Real NVP. In *International Conference on Learning Representations*, 2017.
- Esteban Tabak and Cristina Turner. A family of non-parametric density estimation algorithms. *Communications on Pure and Applied Mathematics*, 66(2):145–164, 2013.
- Ivan Kobyzev, Simon Prince, and Marcus Brubaker. Normalizing flows: an introduction and review of current methods. *IEEE Transactions on Pattern Analysis and Machine Intelligence*, 43(11):3964–3979, 2021.
- Tim Salimans and David Knowles. Fixed-form variational posterior approximation through stochastic linear regression. *Bayesian Analysis*, 8(4):837–882, 2013.
- Diederik Kingma and Max Welling. Auto-encoding variational Bayes. In *International Conference on Learning Representations*, 2014.
- Tanja Eisner, Bálint Farkas, Markus Haase, and Rainer Nagel. *Operator Theoretic Aspects of Ergodic Theory*. Graduate Texts in Mathematics. Springer, 2015.
- Karma Dajani and Sjoerd Dirksin. A simple introduction to ergodic theory, 2008. URL: <https://webspace.science.uu.nl/kraai101/lecturenotes2009.pdf>.
- George Birkhoff. Proof of the ergodic theorem. *Proceedings of the National Academy of Sciences*, 17(12):656–660, 1931.
- Sergio Verdú. Total variation distance and the distribution of the relative information. In *IEEE Information Theory and Applications Workshop*, 2014.
- Radford Neal. *Bayesian Learning for Neural Networks*. Lecture Notes in Statistics, No. 118. Springer-Verlag, 1996.
- Radford Neal. How to view an MCMC simulation as permutation, with applications to parallel simulation and improved importance sampling. *arXiv:1205.0070*, 2012.
- Iain Murray and Lloyd Elliott. Driving Markov chain Monte Carlo with a dependent random stream. *arXiv:1204.3187*, 2012.
- Heikki Haario, Eero Saksman, and Johanna Tamminen. An adaptive Metropolis algorithm. *Bernoulli*, pages 223–242, 2001.
- Radford Neal. Slice sampling. *The Annals of Statistics*, 31(3):705–767, 2003.
- Kirill Neklyudov, Max Welling, Evgenii Egorov, and Dmitry Vetrov. Involutive MCMC: a unifying framework. In *International Conference on Machine Learning*, 2020.

- Span Spanbauer, Cameron Freer, and Vikash Mansinghka. Deep involutive generative models for neural MCMC. *arXiv:2006.15167*, 2020.
- Kôzaku Yosida. Mean ergodic theorem in Banach spaces. *Proceedings of the Imperial Academy*, 14(8):292–294, 1938.
- Shizuo Kakutani. Iteration of linear operations in complex Banach spaces. *Proceedings of the Imperial Academy*, 14(8):295–300, 1938.
- Frigyes Riesz. Some mean ergodic theorems. *Journal of the London Mathematical Society*, 13(4):274–278, 1938.
- Kai Xu, Hong Ge, Will Tebbutt, Mohamed Tarek, Martin Trapp, and Zoubin Ghahramani. Advancedhmc.jl: A robust, modular and efficient implementation of advanced HMC algorithms. In *Symposium on Advances in Approximate Bayesian Inference*, 2020.
- Tor Erlend Fjelde, Kai Xu, Mohamed Tarek, Sharan Yalburgi, and Hong Ge. Bijectors.jl: Flexible transformations for probability distributions. In *Symposium on Advances in Approximate Bayesian Inference*, pages 1–17, 2020.
- David Harrison Jr. and Daniel Rubinfeld. Hedonic housing prices and the demand for clean air. *Journal of Environmental Economics and Management*, 5(1):81–102, 1978.
- U.S. Department of Justice, Federal Bureau of Investigation, Crime in the United States, 1995. URL: <https://ucr.fbi.gov/crime-in-the-u.s/1995>.
- Sérgio Moro, Paulo Cortez, and Paulo Rita. A data-driven approach to predict the success of bank telemarketing. *Decision Support Systems*, 62:22–31, 2014.
- Chuanhai Liu and Donald Rubin. ML estimation of the t distribution using EM and its extensions, ECM and ECME. *Statistica Sinica*, pages 19–39, 1995.
- Kam Hamidieh. A data-driven statistical model for predicting the critical temperature of a superconductor. *Computational Materials Science*, 154:346–354, 2018.

A Proofs

Proposition A.1. *Suppose $X \sim q_{\lambda, N}$, $X_0 \sim q_0$, and $f \in L^2(q_{\lambda, N})$. Then $\mathbb{E}[f(X)] = \mathbb{E}\left[\frac{1}{N} \sum_{n=1}^N f(T^n X_0)\right]$ and $\text{Var}[f(X)] \geq \text{Var}\left[\frac{1}{N} \sum_{n=0}^{N-1} f(T^n X_0)\right]$.*

Proof of Proposition A.1. By the change of variable formula, we can express $\mathbb{E}[f(X)]$ as follows:

$$\mathbb{E}[f(X)] = \frac{1}{N} \sum_{n=0}^{N-1} \int q_0(x) f(T_\lambda^n x) dx = \frac{1}{N} \sum_{n=0}^{N-1} \mathbb{E}[f(T^n X_0)] = \mathbb{E}\left[\frac{1}{N} \sum_{n=1}^N f(T^n X_0)\right]. \quad (6)$$

Then, to compare the variance, it is sufficient to show $\mathbb{E}[f^2(X)] \geq \mathbb{E}\left[\left(\frac{1}{N} \sum_{n=1}^N f(T^n X_0)\right)^2\right]$. Notice that by Jensen's inequality, we have

$$\mathbb{E}\left[\left(\frac{1}{N} \sum_{n=1}^N f(T^n X_0)\right)^2\right] \leq \mathbb{E}\left[\frac{1}{N} \sum_{n=1}^N f^2(T^n X_0)\right] = \mathbb{E}[f^2(X)].$$

The last equality is by the same application of change of variable formula as Eq. (6). \square

Proof of Theorem 3.1. Since setwise convergence implies weak convergence, we will focus on proving setwise convergence. We have that $q_{\lambda, N}$ converges setwise to π if and only if for all measurable bounded $f : \mathcal{X} \rightarrow \mathbb{R}$,

$$\mathbb{E}f(X_N) \rightarrow \mathbb{E}f(X), \quad X_N \sim q_{\lambda, N}, \quad X \sim \pi.$$

The proof proceeds by directly analyzing $\mathbb{E}f(X_N)$:

$$\begin{aligned} \mathbb{E}f(X_N) &= \int f(x) q_{\lambda, N}(dx) \\ &= \frac{1}{N} \sum_{n=0}^{N-1} \int f(x) (T_\lambda^n q_0)(dx) \\ &= \frac{1}{N} \sum_{n=0}^{N-1} \int f(T_\lambda^n x) q_0(dx) \\ &= \int \frac{1}{N} \sum_{n=0}^{N-1} f(T_\lambda^n x) q_0(dx). \end{aligned}$$

Since $q_0 \ll \pi$, by the Radon-Nikodym theorem, there exists a density of q_0 with respect to π , so

$$\mathbb{E}f(X_N) = \int \frac{1}{N} \sum_{n=0}^{N-1} f(T_\lambda^n x) \frac{dq_0}{d\pi}(x) \pi(dx).$$

By the pointwise ergodic theorem (Theorem 2.3), $f_N(x) = \frac{1}{N} \sum_{n=0}^{N-1} f(T_\lambda^n x)$ converges pointwise π -a.e. to $\int f d\pi$; and because f is bounded, f_N is uniformly bounded for all $N \in \mathbb{N}$. Hence by the Lebesgue dominated convergence theorem,

$$\begin{aligned} \lim_{N \rightarrow \infty} \mathbb{E}f(X_N) &= \lim_{N \rightarrow \infty} \int \frac{1}{N} \sum_{n=0}^{N-1} f(T_\lambda^n x) \frac{dq_0}{d\pi}(x) \pi(dx) \\ &= \int \left(\int f d\pi \right) \frac{dq_0}{d\pi}(x) \pi(dx) \\ &= \left(\int f d\pi \right) \cdot 1 = \mathbb{E}f(X). \end{aligned}$$

\square

Theorem A.2 (Mean ergodic theorem in Banach spaces [Yosida, 1938; Kakutani, 1938; Riesz, 1938; Eisner et al., 2015, Theorem 8.5]). *Let T be a bounded linear operator on a Banach space E , define the operator*

$$A_N = \frac{1}{N} \sum_{n=0}^{N-1} T^n,$$

and let

$$\text{fix}(T) = \{v \in E : Tv = v\} = \ker(I - T).$$

Suppose that $\sup_{N \in \mathbb{N}} \|A_N\| < \infty$ and that $\frac{1}{N}T^N v \rightarrow 0$ for all $v \in E$. Then the subspace

$$V = \left\{ v \in E : \lim_{N \rightarrow \infty} A_N v \text{ exists} \right\}$$

is closed, T -invariant, and decomposes into a direct sum of closed subspaces

$$V = \text{fix}(T) \oplus \overline{\text{range}}(I - T).$$

The operator $T|_V$ on V is mean ergodic. Furthermore, the operator

$$A : V \rightarrow \text{fix}(T) \quad Av = \lim_{N \rightarrow \infty} A_N v$$

is a bounded projection with kernel $\ker(A) = \overline{\text{range}}(I - T)$ and $AT = A = TA$.

Proof of Theorem 3.2. Denote μ to be the Lebesgue measure on \mathbb{R}^d , and consider the Banach space $L^1(\mu)$ and linear operator T on $L^1(\mu)$ defined by

$$Tf = \frac{f(T^{-1}(x))}{J(T^{-1}(x))},$$

where $J(x)$ is the Jacobian determinant of $T(x)$. We suppress λ subscripts for brevity, and note the slight abuse of notation involving the same symbol for $T : \mathcal{X} \rightarrow \mathcal{X}$ the associated operator. By a simple change of variables,

$$\|Tf\|_1 = \int |Tf(x)|\mu(dx) = \int |f(x)|\mu(dx) = \|f\|_1,$$

and so T is bounded with $\|T\| = 1$. Hence $\frac{1}{N}T^N f \rightarrow 0$ for all $f \in L^1(\mu)$, and if we define the operator

$$\forall N \in \mathbb{N}, \quad A_N = \frac{1}{N} \sum_{n=0}^{N-1} T^n,$$

we have that $\sup_{N \in \mathbb{N}} \|A_N\| \leq 1$. Therefore by the mean ergodic theorem in Banach spaces [Yosida, 1938; Kakutani, 1938; Riesz, 1938; Eisner et al., 2015, Theorem 8.5], we have that

$$A : E \rightarrow \text{fix}(T) \quad Af = \lim_{N \rightarrow \infty} A_N f$$

where $E = \{f \in L^1(\mu) : \lim_{N \rightarrow \infty} A_N f \text{ exists}\}$. (Eisner et al., 2015, Theorem 8.20) guarantees that $E = L^1(\mu)$ as long as the weak limit of $A_N f$ exists for each $f \in L^1(\mu)$. Note that since μ is σ -finite, the dual space of $L^1(\mu)$ is the set of linear functionals

$$f \mapsto \int f(x)\phi(x)\mu(dx), \quad \phi \in L^\infty(\mu).$$

So therefore we have that $E = L^1(\mu)$ if for each $f \in L^1(\mu)$, there exists a $g \in L^1(\mu)$ such that

$$\forall \phi \in L^\infty(\mu), \quad \int (A_N f)(x)\phi(x)\mu(dx) \rightarrow \int g(x)\phi(x)\mu(dx).$$

The same technique using a transformation of variables and the pointwise ergodic theorem from the proof of Theorem 3.1 provides the desired weak convergence. Therefore we have L^1 convergence to $\text{fix}(T)$ and hence total variation convergence to an element of $\text{fix}(T)$. Since $q_0 \ll \pi$, Theorem 3.1 guarantees weak convergence to π ; and since we know $A_N f \rightarrow \text{fix}(T)$ and $\pi \in \text{fix}(T)$, we have that $D_{\text{TV}}(q_{\lambda, N}, \pi) \rightarrow 0$. \square

Proposition A.3 ((Verdú, 2014, Theorem 7)). *Suppose q, π are two probability distributions on \mathcal{X} such that $q \ll \pi$ and both have a density with respect to a common base measure. If*

$$\alpha = \sup_{x \in \mathcal{X}} \frac{q(x)}{\pi(x)} < \infty,$$

then

$$D_{\text{TV}}(q, \pi) \geq \frac{\alpha - 1}{2\alpha \log \alpha} D_{\text{KL}}(q|\pi).$$

Proof. We provide a proof for completeness. The KL divergence is

$$D_{\text{KL}}(q||\pi) = \int q(x) \log \frac{q(x)}{\pi(x)} dx = \int \pi(x) \frac{q(x)}{\pi(x)} \log \frac{q(x)}{\pi(x)} dx.$$

Note that $\alpha \geq 1$ by definition, and that

$$\forall y \in [0, \alpha], \quad \frac{\alpha \log \alpha}{\alpha - 1} |y - 1| \geq y \log y.$$

Therefore

$$D_{\text{KL}}(q||\pi) \leq \frac{\alpha \log \alpha}{\alpha - 1} \int \pi(x) \left| \frac{q(x)}{\pi(x)} - 1 \right| dx = \frac{2\alpha \log \alpha}{\alpha - 1} \frac{1}{2} \int |q(x) - \pi(x)| dx = \frac{2\alpha \log \alpha}{\alpha - 1} D_{\text{TV}}(q, \pi).$$

□

B Memory efficient ELBO estimation

Algorithm 4 `DensityTriple(x)`: Evaluate $T_\lambda^{-N+1}(x)$, $q_{\lambda,N}(x)$, and $\prod_{j=1}^{N-1} J_\lambda(T_\lambda^{-j}x)$ with $O(N)$ -time, $O(1)$ -memory

Require: location x , reference distribution q_0 , flow map T_λ , Jacobian J_λ , number of steps N

```

L ← 0
w ← q0(x)
for n = 1, ..., N - 1 do
  x ← Tλ-1(x)
  L ← L + log Jλ(x)
  w ← LogSumExp(w, log q0(x) - L)
end for
w ← w - log N
return x, exp(w), exp(L)

```

Algorithm 5 `EstELBO(λ, N)`: Estimate the ELBO for $q_{\lambda,N}$ in $O(N)$ -time, $O(1)$ -memory.

Require: reference q_0 , unnormalized target p , flow map T_λ , Jacobian J_λ , number of flow steps N

```

x ← Sample(q0)
x', z, J ← DensityTriple(x)
f ← log p(x)
g ← log z
for n = 1, ..., N - 1 do
  q̄ ← (1/N) q0(x') / J
  Jn-1 ← Jλ(x)
  z ← (z - q̄) / Jn-1
  x ← Tλ(x)
  z ← z + (1/N) q0(x)
  f ← f + log p(x)
  g ← g + log z
  if n < N - 1 then
    J ← J · Jn-1 / Jλ(x')
  end if
  x' ← Tλ(x')
end for
 $\widehat{\text{ELBO}}(\lambda, N) \leftarrow \frac{1}{N}(f - g)$ 
return  $\widehat{\text{ELBO}}(\lambda, N)$ 

```

C Hamiltonian flow pseudocode

Algorithm 6 Compute $T_{\lambda,\epsilon}$ and its Jacobian $J_{\lambda,\epsilon}$ for Hamiltonian flow with leapfrog integrator

Require: initial state $x \in \mathcal{X}$, $\rho \in \mathbb{R}^d$, $u \in [0, 1]$, step size ϵ , shift $\xi \in \mathbb{R}$, pseudorandom shift $z(\cdot, \cdot)$

```

 $x_0, \rho_0 \leftarrow x, \rho$ 
for  $\ell = 1, \dots, L$  do
     $x_\ell, \rho_\ell \leftarrow \hat{H}_\epsilon(x_{\ell-1}, \rho_{\ell-1})$ 
end for
 $x', \rho' \leftarrow x_L, \rho_L$ 
 $u' \leftarrow u + \xi \pmod{1}$ 
for  $i = 1, \dots, d$  do
     $\rho''_i \leftarrow R^{-1}(R(\rho'_i) + z(x'_i, u')) \pmod{1}$ 
end for
 $J \leftarrow m(\rho')/m(\rho'')$ 
return  $(x', \rho'', u'), J$ 

```

D Extensions

Tunable reference So far we have assumed that the reference distribution q_0 for the flow is fixed. Given that q_0 is often quite far from the target π , this forces the variational flow to spend some of its steps just moving the bulk of the mass to π . But this can be accomplished much easier with, say, a simple linear transformation that efficiently allows large global moves in mass. For example, if $q_0 = \mathcal{N}(0, I)$, we can include a map M_θ

$$q_{\lambda,N} = \frac{1}{N} \sum_{n=0}^{N-1} T_\lambda^n M_\theta q_0,$$

where $M_\theta(x) = \theta_1 x + \theta_2$, where $\theta_1 \in \mathbb{R}^{d \times d}$ and $\theta_2 \in \mathbb{R}^d$. Note that it is possible to optimize the reference and flow jointly, or to optimize the reference distribution by itself first and then use that fixed reference in the flow optimization.

Automated burn-in A common practice in MCMC is to throw away a first fraction of the states in the sequence to ensure that the starting sample is in a high probability region of the target distribution, thus reducing the bias from initialization (“burn-in”). Usually one needs a diagnostic to check when burn-in is completed. In the case of `ERGFlow`, we can monitor the burn-in phase in a principled way by evaluating the ELBO. Once the flow is trained, the variational distribution with M burn-in samples is simply

$$q_{\lambda,M,N} = \frac{1}{N-M} \sum_{n=M}^{N-1} T_\lambda^n q_0,$$

We can easily optimize this by estimating the ELBOs for $M = 1, \dots, N$.

Mixed flows One can build multiple flows starting from multiple different initial reference distributions; when the posterior is multimodal, it may be the case that some of these flows converge to different modes but do not mix across modes. In this scenario, it can be helpful to mix several flows, i.e., build an approximation of the form

$$q_{\lambda,N}^* = \sum_{k=1}^K w_k (q_{\lambda,N})_k, \quad \sum_{k=1}^K w_k = 1.$$

Because each component flow provides access to i.i.d. samples and density evaluation, `ERGFlow` provides the ability to optimize the weights by maximizing the ELBO (i.e., minimizing the KL divergence).

E Additional experimental details

In this section, we provide details for each experiment presented in the main text, as well as additional results regarding numerical stability and a high-dimensional synthetic experiment. Aside from the univariate synthetic example, all examples include a pseudotime shift step with $\xi = \pi/16$, and a momentum refreshment with $z(x, u) = 0.5 \sin(2x + u) + 0.5$. For the kernel Stein discrepancy, we use a IMQ kernel $k(x, y) = (c^2 + \|x - y\|_2^2)^\beta$ with $\beta = -0.5, c = 1$, the same setting as in (Gorham and Mackey, 2017). For all experiments, unless otherwise stated, NUTS uses 20,000 steps for adaptation, targeting at an average acceptance ratio 0.7, and generates 5,000 samples for KSD estimation. The KSD for `ERGFlow` is estimated using 2,000 samples. As for NUTS, we use the Julia package

AdvancedHMC.jl (Xu et al., 2020) with all default settings. The ESS is computed using the R package `mcmcse`, which is based on batch mean estimation. We implement all NFs using the Julia package `Bijectors.jl` (Fjelde et al., 2020). The flow layers of `PlanarFlow` and `RadialFlow`, as well as the coupling layers of `RealNVP` are implemented in `Bijectors.jl`. The affine coupling functions of `RealNVP`—a scaling function and shifting function—are both parameterized using fully connected neural networks of three layers, of which the activation function is LeakyReLU and number of hidden units is by default the same dimension as the target distribution, unless otherwise stated.

E.1 Univariate synthetic examples

The three target distributions tested in this experiment were

- normal: $\mathcal{N}(2, 2^2)$,
- synthetic Gaussian mixture: $0.5\mathcal{N}(-3, 1.5^2) + 0.3\mathcal{N}(0, 0.8^2) + 0.2\mathcal{N}(3, 0.8^2)$, and
- Cauchy: $\text{Cauchy}(0, 1)$.

For all three examples, we use a momentum refreshment without introducing the pseudotime variable; this enables us to plot the full joint density of $(x, \rho) \in \mathbb{R}^2$:

$$\rho'' \leftarrow R_{\text{Lap}}^{-1}(R_{\text{Lap}}(\rho') + (\sin(2x') + 1)/2 \pmod{1}).$$

For the three examples, we used the leapfrog stepsize $\epsilon = 0.05$ and run $L = 50$ leapfrogs between each refreshment. For both the Gaussian and Gaussian mixture targets, we use 100 refreshments. In the case of the Cauchy, we used 1,000 refreshments.

E.2 Multivariate synthetic examples

The three target distributions tested in this experiment were

- the banana distribution (Haario et al., 2001):

$$y = \begin{bmatrix} y_1 \\ y_2 \end{bmatrix} \sim \mathcal{N}\left(0, \begin{bmatrix} 100 & 0 \\ 0 & 1 \end{bmatrix}\right), \quad x = \begin{bmatrix} y_1 \\ y_2 + by_1^2 - 100b \end{bmatrix}, \quad b = 0.1;$$

- Neals’ funnel (Neal, 2003):

$$x_1 \sim \mathcal{N}(0, \sigma^2), \quad x_2 | x_1 \sim \mathcal{N}\left(0, \exp\left(\frac{x_1}{2}\right)\right), \quad \sigma^2 = 36;$$

- a cross-shaped distribution: in particular, a Gaussian mixture of the form

$$x \sim \frac{1}{4}\mathcal{N}\left(\begin{bmatrix} 0 \\ 2 \end{bmatrix}, \begin{bmatrix} 0.15^2 & 0 \\ 0 & 1 \end{bmatrix}\right) + \frac{1}{4}\mathcal{N}\left(\begin{bmatrix} -2 \\ 0 \end{bmatrix}, \begin{bmatrix} 1 & 0 \\ 0 & 0.15^2 \end{bmatrix}\right) \\ + \frac{1}{4}\mathcal{N}\left(\begin{bmatrix} 2 \\ 0 \end{bmatrix}, \begin{bmatrix} 1 & 0 \\ 0 & 0.15^2 \end{bmatrix}\right) + \frac{1}{4}\mathcal{N}\left(\begin{bmatrix} 0 \\ -2 \end{bmatrix}, \begin{bmatrix} 0.15^2 & 0 \\ 0 & 1 \end{bmatrix}\right);$$

- and a warped Gaussian distribution

$$y = \begin{bmatrix} y_1 \\ y_2 \end{bmatrix} \sim \mathcal{N}\left(0, \begin{bmatrix} 1 & 0 \\ 0 & 0.12^2 \end{bmatrix}\right), \quad x = \begin{bmatrix} \|y\|_2 \cos(\text{atan2}(y_2, y_1) - \frac{1}{2}\|y\|_2) \\ \|y\|_2 \sin(\text{atan2}(y_2, y_1) - \frac{1}{2}\|y\|_2) \end{bmatrix},$$

where $\text{atan2}(y, x)$ is the angle, in radians, between the positive x axis and the ray to the point (x, y) .

For each target distribution we used a flow with 1,000 refreshments; between each refreshment we used 50 leapfrog steps for the banana distribution, 60 for the cross distribution, and 80 for the funnel and warped Gaussian. Note that in all four examples, we individually tuned the step size ϵ by maximizing the estimated ELBO, as shown in Fig. 6a. Fig. 6b also demonstrates how the ELBO varies versus the number of refreshments N . For small step sizes ϵ , the discretized Hamiltonian dynamics approximates the continuous dynamics, and the ELBO generally increases with N indicating convergence to the target. For larger step sizes ϵ , the ELBO increases to a peak and then decreases, indicating that the discretized dynamics do not exactly target the desired distribution.

Fig. 7 shows why we opted to use a Laplace momentum distribution as opposed to a Gaussian momentum. In particular, the numerical error of composing $T_\lambda^K \circ T_\lambda^{-K}$ and $T_\lambda^{-K} \circ T_\lambda^K$ (denoted as “Bwd” and “Fwd” in the legend, respectively) indicate that the flow using the Laplace momentum is more reliably invertible for larger numbers of refreshments than the flow with a Gaussian momentum. This is largely due to the fact that the normal has very light tails; for example, for large momentum values in the right tail, the CDF is ≈ 1 , which gets rounded to exactly 1 in floating point representation. Note that our implementation of the CDF and inverse CDF was fairly naïve; more stable computation could be achieved with more care taken to prevent rounding.

Finally, Fig. 8 provides a more comprehensive set of sample histograms for these experiments, showing the x -, ρ -, and u -marginals. It is clear that `ErgFlow` generates samples for each variable reliably from the target marginal.

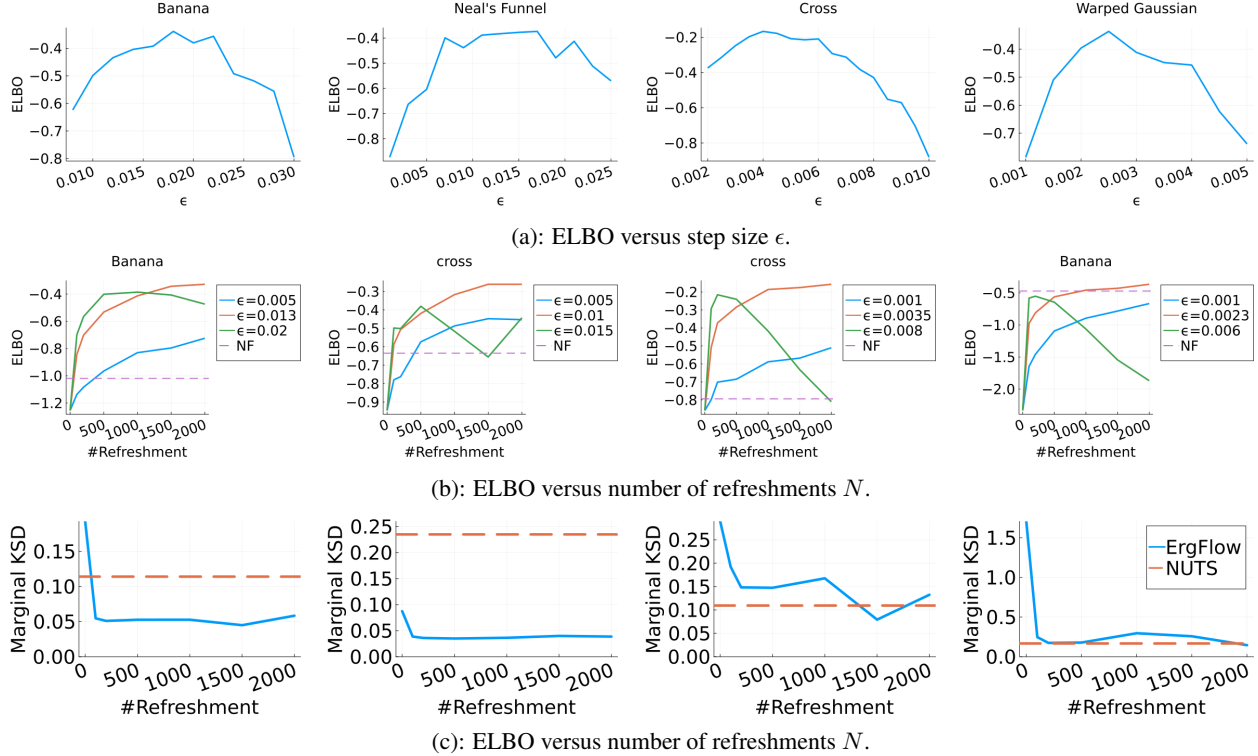


Figure 6: Tuning for the four multivariate synthetic examples, and KSD comparison to NUTS of the tuned ErgFlow.

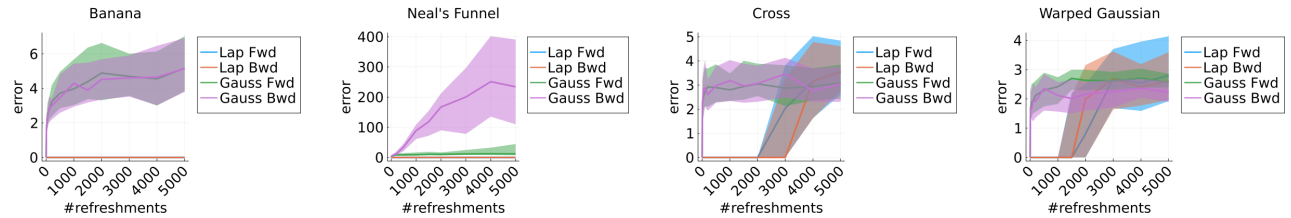


Figure 7: Stability of composing $T_\lambda^{-K} \circ T_\lambda^K$ (Fwd) and $T_\lambda^K \circ T_\lambda^{-K}$ (Bwd) for the four multivariate experiments with flows constructed using Gaussian (Gauss) and Laplace (Lap) momentum distributions. The vertical axis shows the 2-norm error of reconstructing (x, ρ, u) sampled from q_0 ; the horizontal axis shows increasing numbers of refreshments K . The lines indicate the median, and error regions indicate 25th to 75th percentile for 100 independent samples.

E.3 Higher-dimensional synthetic experiment

We also tested two higher dimensional Neal's funnel target distributions of $x \in \mathbb{R}^d$ where $d = 5, 20$. In particular, we used the target distribution

$$x_1 \sim \mathcal{N}(0, \sigma^2), \quad \text{and} \quad \forall i \in \{2, \dots, d\}, \quad x_i | x_1 \stackrel{\text{i.i.d.}}{\sim} \mathcal{N}\left(0, \exp\left(\frac{x_1}{2}\right)\right),$$

with $\sigma^2 = 36$. We use 80 leapfrogs between refreshments and $\epsilon = 0.0009$ when $d = 5$, and 100 leapfrogs between refreshments and $\epsilon = 0.001$ when $d = 20$ (Figs. 9a and 9c shows the ELBO comparison used to tune the step size ϵ). Figs. 9b and 9d confirm via the KSD that the method performs as well as NUTS in higher-dimensional cases.

E.3.1 Additional experiments for synthetic examples

In this section, we provide additional comparisons on sample quality and sampling efficiency of ErgFlow, using all four synthetic examples in Appendix E.2, against NUTS, HMC, and a generic normalizing flow method—planar flow (NF) (Rezende and Mohamed, 2015b). For this set of experiments, all of the settings for ErgFlow are the same as outlined in Appendix E.2. HMC uses the same leapfrog step size and number of leapfrogs steps (between refreshments) as ErgFlow. For NF, 5 Planar layers (Rezende and Mohamed, 2015b) that contain 40 parameters to be optimized (4 translation parameters and 4 scaling parameters per layer) are used unless otherwise stated. We train NF using ADAM until convergence (100,000 iterations except where otherwise noted) with the initial step size set

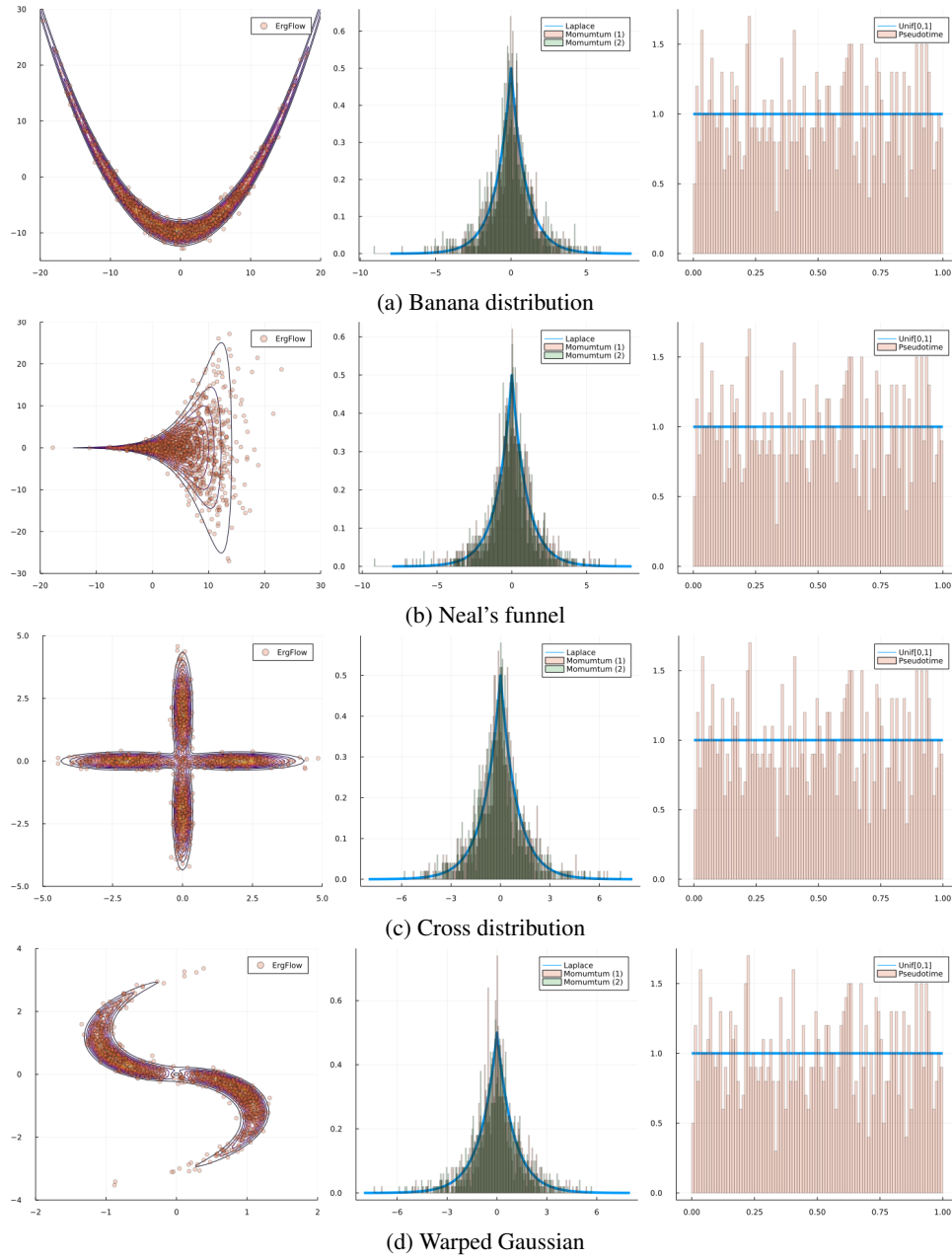


Figure 8: Scatter plots and histograms for the x -, ρ -, and u -marginals in the four synthetic experiments.

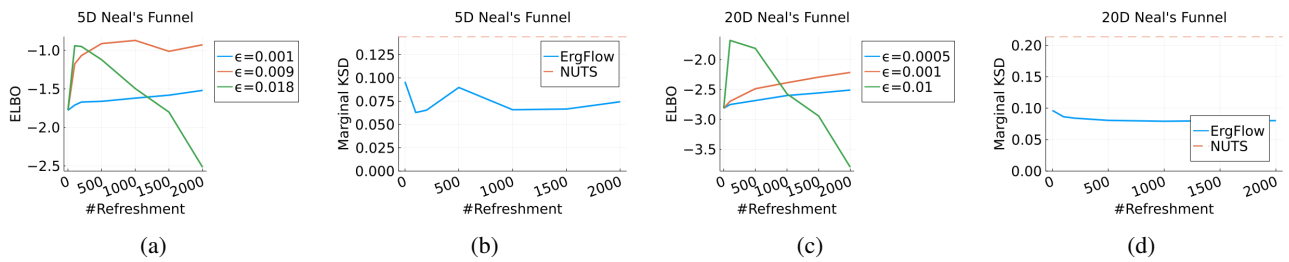
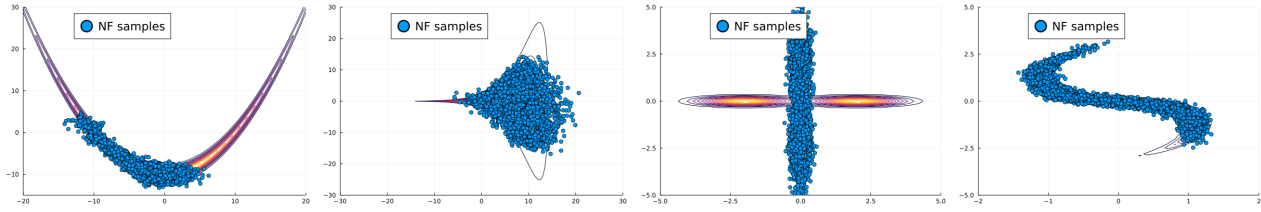
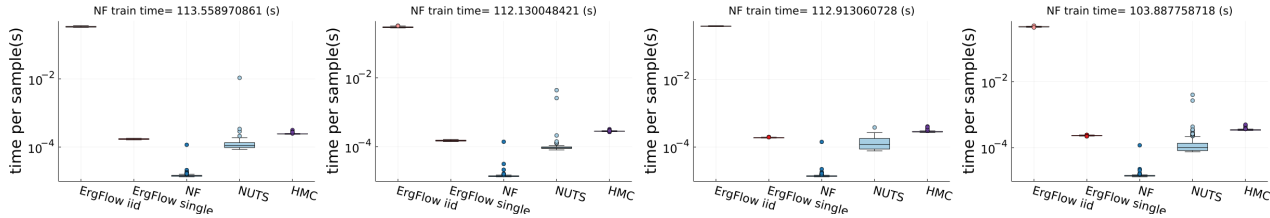


Figure 9: ELBO versus step size (9a,9c) and KSD comparison with NUTS (9b,9d) for the 5- and 20-dimensional Neal's funnel examples.

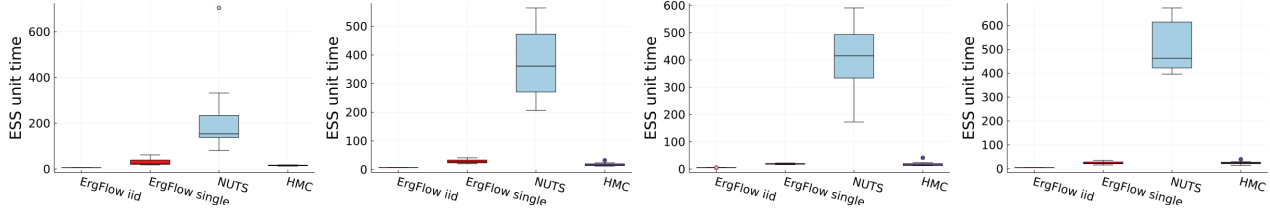


(b): Scatter plot of 5000 i.i.d. samples generated from trained NF.

Figure 10: Performance of NF for the four multivariate synthetic examples.



(a): Sampling time comparison to NF, NUTS, and HMC (100 trials).



(b): Per second ESS comparison to NUTS and HMC (100 trials).

Figure 11: Time results for four multivariate synthetic examples: from left to right, each column corresponds to Banana, Neal's funnel, Cross, and warped Gaussian respectively.

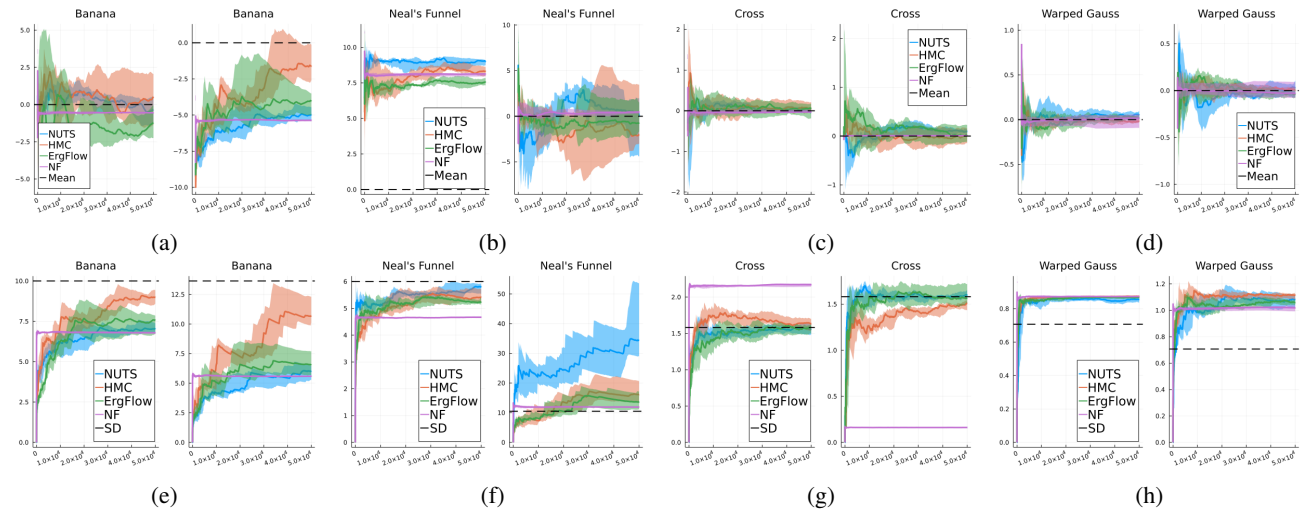


Figure 12: Streaming mean and standard deviation (SD) estimation (50,000 samples) for four 2-dimensional synthetic distributions. For each distribution, the two plots on the top row correspond to the two marginal means, and the two plots on the bottom row correspond to the two marginal SDs. Each plot shows the evolution of coordinate-wise mean/SD estimates, using samples from ErgFlow single (green), NUTS (blue), HMC (red), and NF (purple); black dashed line indicates the true target mean/SD, which is estimated using 50,000 samples from the actual synthetic target distribution. The lines indicate the median, and error regions indicate 25th to 75th percentile from 10 runs.

to 0.001. And at each step, 10 samples are used for gradient estimation. The initial distribution for `ErgFlow` and `NF` is set to be the mean-field Gaussian approximation, and `HMC` and `NUTS` are initialized using the learned mean of the mean-field Gaussian approximation. All parameters in `NF` are initialized using random samples from the standard Gaussian distribution.

Fig. 6b compares the joint ELBO values across various leapfrog step sizes for `ErgFlow` against that of `NF`. We see that in all four examples, `NF` produces a smaller ELBO than `ErgFlow` with a reasonable step size, which implies a lower quality target approximation. Indeed, Fig. 10a shows that the trained `NF`s fail to capture the shape of the target distributions. Although one may expect the performance of `NF` to improve if it were given more layers, we will show that this is not the case in a later paragraph.

Fig. 11a compares the sampling efficiency of `ErgFlow` against `NUTS`, `HMC`, and `NF`. We see that `ErgFlow iid` is the slowest, because each sample is generated by passing through the entire flow. However, we see that by taking all intermediate samples as in `ErgFlow single`, we can generate samples just as fast as `NUTS` and `HMC`. On the other hand, while `NF` is fastest for sampling, it requires roughly 2 minutes for training, which alone allows `ErgFlow single`, `NUTS`, and `HMC` to generate over 1 million samples in these examples. A more detailed discussion about this trade-off for `NF` is presented later.

Fig. 11b further shows the computational efficiency in terms of effective samples size (ESS) per second. The smaller per second ESS of `ErgFlow iid` is due to its slower sampling time. However, we emphasize that these samples are i.i.d.. `NUTS` achieves a much higher per second ESS because of the much longer trajectories it produces (it only terminates once it detects a ‘‘U-turn’’). This is actually an illustration of a limitation of the ESS per unit time as a measurement of performance. Because `NUTS` generates longer trajectories, it has a lower sample autocorrelation and a higher ESS; but Fig. 12 shows that the actual estimation performance of `NUTS` is comparable to the other methods. Note that it is also possible to incorporate the techniques used in `NUTS` to our method, which we leave for future work.

As mentioned above, ESS mainly serves as a practical index for the relative efficiency of using a sequence of dependent samples, as opposed to independent samples, to estimate certain summary statistics of the target distribution. In this case, `ErgFlow single` can be very useful. Fig. 12 demonstrate the performance of `ErgFlow single`, `NUTS`, `HMC`, and `NF` when estimating the coordinate-wise means and standard deviations (SD) of target distributions. We see that `ErgFlow single`, `NUTS`, and `HMC` generally show similar performance in terms of convergence speed and estimation precision. While `NF` converges very quickly due to i.i.d. sampling, it does seem to struggle more at identifying the correct statistics, particularly the standard deviation, given its limited approximation quality. It is worth noting that, unlike `ErgFlow` and general MCMC methods, sample estimates of target summaries obtained from `NF` are typically not asymptotically exact, as the sample quality is fundamentally limited by the choice of variational family and how well the flow is trained.

Finally, we provide an additional set of results for `NF` (Fig. 13), examining its performance as we increase the number of planar layers (5, 10, 20, 50). All settings for `NF` are identical to the above, except that we increase the optimization iteration to 500,000 to ensure the convergence of flows with increased numbers of layers. As demonstrated in the second and third column of Fig. 13, both training time and sampling time scale with the number of layers roughly linearly. Although a trained `NF` is still generally faster in sample generation (see also Fig. 11a), for these synthetic examples with 4-dimensional joint target distributions, training time can take up to 30 minutes. More importantly, the corresponding target approximations of `NF` are still not as good as those of `ErgFlow` in all four examples, even when we increase the number of layers to 50, which corresponds to optimizing 400 parameters from the flow. One may also notice from Fig. 13 that a more complex normalizing flow does not necessarily lead to better performance. This is essentially because the (usually non-convex) KL optimization problem of standard `NF` becomes more complex to solve as the flow becomes more flexible. As a result, even though theoretically, `NF` becomes more expressive with more layers, there is no guarantee on how well it approximates the target distribution. In contrast, `ErgFlow` is optimization-free and is asymptotically exact—with a proper choice of hyper-parameter, more computation typically leads to better performance (Fig. 6b). With the 30 minutes training time of `NF`, `ErgFlow iid` can generate 18,000 i.i.d. samples and `ErgFlow single` can generate over 10 million i.i.d. samples, both of which are more than sufficient for most estimations under these target distributions.

E.4 Real data examples

All settings for `ErgFlow`, `NUTS` and `HMC` are identical to those in synthetic examples. All `NF`s are trained using ADAM for 200,000 iterations with initial step size set to be 0.001.

E.4.1 Bayesian linear regression

We consider two Bayesian linear regression problems, with both a standard normal prior and a heavy tail prior using two sets of real data. The two statistical models take the following form:

$$\log \sigma^2 \stackrel{\text{i.i.d.}}{\sim} \mathcal{N}(0, 1), \quad y_j \mid \beta, \sigma^2 \stackrel{\text{indep}}{\sim} \mathcal{N}\left(x_j^T \beta, \sigma^2\right)$$

$$\text{Normal: } \beta \stackrel{\text{i.i.d.}}{\sim} \mathcal{N}(0, 1) \quad \text{Cauchy: } \beta \stackrel{\text{i.i.d.}}{\sim} \text{Cauchy}(0, 1)$$

where y_j is the response and $x_j \in \mathbb{R}^p$ is the feature vector for data point j . For linear regression problem with a normal prior, we use the Boston housing prices dataset (Harrison Jr. and Rubinfeld, 1978). Dataset available in the `MLDatasets` Julia package at <https://github.com/JuliaML/MLDatasets.jl>. containing $J = 506$ suburbs/towns in the Boston area; the goal is to use suburb information to predict the median house price. We standardize all features and responses. For linear regression with a heavy-tail prior, we use the communities and crime dataset (com, 1995), available at <http://archive.ics.uci.edu/ml/datasets/Communities+and+Crime>. The original dataset contains 122 attributes that potentially connect to crime; the goal is to predict per-capita violent crimes using the information of the community, such as the median family income, per capita number of police officers, and etc. For the data preprocessing, we drop observations with missing values, and using Principle component analysis for feature dimension reduction; we selected 50

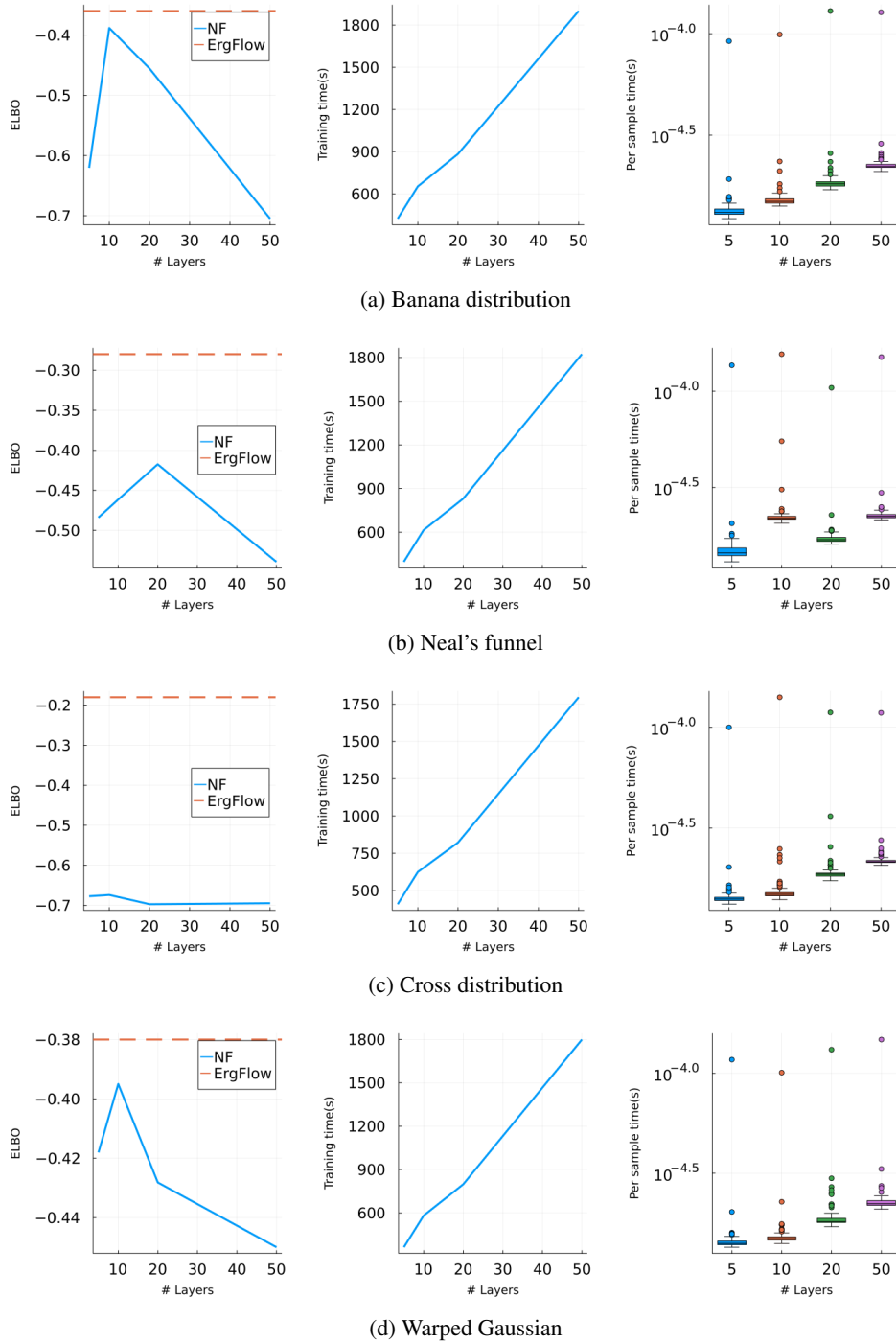


Figure 13: Additional NF results with number of planar layers (5, 10, 20, 50). First column shows the ELBO value. Each ELBO is estimated using 2000 i.i.d. samples from trained flow. The second and third columns correspond to the training time and per-sample time (100 trials) of NF given increasing planar layers.

principle components with leading eigenvalues. The posterior dimensions of the two linear regression inference problems are 15 and 52, respectively.

E.4.2 Bayesian generalized linear regression

We then consider two Bayesian generalized linear regression problems—a hierarchical logistic regression and a poisson regression:

Logis. Reg.: $\alpha \sim \text{Gam}(1, 0.01), \beta \mid \alpha \sim \mathcal{N}(0, \alpha^{-1}I),$

$$y_j \mid \beta \stackrel{\text{indep}}{\sim} \text{Bern} \left(\frac{1}{1 + e^{-x_j^T \beta}} \right),$$

Poiss. Reg.: $\beta \sim \mathcal{N}(0, I),$

$$y_j \mid \beta \stackrel{\text{indep}}{\sim} \text{Pois} \left(\log \left(1 + e^{-x_j^T \beta} \right) \right),$$

For logistic regression, we use a bank marketing dataset (Moro et al., 2014) downsampled to $J = 400$ data points. Original dataset is available at <https://archive.ics.uci.edu/ml/datasets/bank+marketing>. the goal is to use client information to predict whether they subscribe to a term deposit. We include 8 features from the bank marketing dataset (Moro et al., 2014): client age, marital status, balance, housing loan status, duration of last contact, number of contacts during campaign, number of days since last contact, and number of contacts before the current campaign. For each of the binary variables (marital status and housing loan status), all unknown entries are removed. All features of the dataset are also standardized. Hence the posterior dimension of the logistic regression problem is 9 and the overall (x, ρ, u) state dimension of the logistic regression inference problems are 19.

For Poisson regression problem, we use an airport delays dataset with 15 features and $J = 500$ data points (subsampled), resulting a 16-dimensional posterior distribution. The airport delays dataset was constructed using flight delay data from <http://stat-computing.org/dataexpo/2009/the-data.html> and historical weather information from <https://www.wunderground.com/history/>. relating daily weather information to the number of flights leaving an airport with a delay of more than 15 minutes. All features are standardized as well.

E.4.3 Bayesian Student-t regression

We also consider a Bayesian Student-t regression problem, of which the posterior distribution is heavy-tail. The Student-t regression model is as follows:

$$y_i \mid X_i, \beta \sim \mathcal{T}_5(X_i^T \beta, 1), \quad \beta \stackrel{\text{i.i.d.}}{\sim} \text{Cauchy}(0, 1).$$

In this example, we use the creatinine dataset (Liu and Rubin, 1995), containing a clinical trial on 34 male patients with 3 covariates. Original dataset is available in <https://github.com/faosorios/heavy/blob/master/data/creatinine.rda>. The 3 covariates consist of body weight in kg(WT), serum creatininte concentration (SC), and age in years. The goal is to predict the endogenous cretinine clearance (CR) using these covariates. We apply the data transformation recommended by Liu and Rubin (1995) by transferring response into $\log(\text{CR})$, and transferring covariats into $\log(\text{WT})$, $\log(\text{SC})$, $\log(140 - \text{age})$.

E.4.4 Bayesian sparse regression

Finally, we compare the methods on the Bayesian sparse regression problem applied to two datasets: a prostate cancer dataset containing 9 covariates and 97 observations, and a superconductivity dataset (Hamidieh, 2018), containing 83 features and 100 observations (subsampled). The prostate cancer dataset is available at <https://hastie.su.domains/ElemStatLearn/datasets/prostate.data>. The superconductivity dataset is available at <https://archive.ics.uci.edu/ml/datasets/superconductivity+data>. The model is as follows:

$$\log \sigma^2 \stackrel{\text{i.i.d.}}{\sim} \mathcal{N}(0, 1), \beta_i \stackrel{\text{i.i.d.}}{\sim} \frac{1}{2} \mathcal{N}(0, \tau_1^2) + \frac{1}{2} \mathcal{N}(0, \tau_2^2),$$

$$y_j \mid \beta, \sigma^2 \stackrel{\text{indep}}{\sim} \mathcal{N} \left(x_j^T \beta, \sigma^2 \right)$$

For both two datasets, we set $\tau_1 = 0.1, \tau_2 = 10$. The resulting posterior dimension for both datasets are 10 and 84 respectively. When data information is weak, the posterior distribution in this model typically contains multiple modes (Xu and Campbell, 2022). We standardize the covariates during the preprocessing procedure for both datasets.

E.4.5 Additional experiments for real data examples

Table 1: Comparison of ELBO between ErgFlow and RealNVP with different number of layers on real data example. Each setting of RealNVP is run in 5 trials. ELBOs of ErgFlow are estimated using 1000 independent trajectories and ELBOs of RealNVP are estimated using 2000 independent samples.

ErgFlow					
	STEPSIZE	#LEAPFROG	#REFRESHMENT	ELBO	#SAMPLE
Lin Reg	0.0005	30	2000	-429.98	1000
Lin Reg Heavy	0.000025	50	2500	117.1	1000
Log Reg	0.002	50	1500	-250.5	1000
Poiss Reg	0.0001	50	2000	82576.9	1000
Student t Reg	0.0008	80	2000	-145.41	1000
Sparse Reg	0.001	30	600	-125.9	1000
Sparse Reg High Dim	0.0012	50	2000	-538.36	2000
RealNVP					
	#LAYER	#HIDDEN	MEDIAN	IQR	#NAN
Lin Reg	5	15	-429.43	(-429.56, -429.42)	0
Lin Reg	10	15	-429.41	(-429.43, -429.36)	1
Lin Reg Heavy	5	52	116.47	(116.34, 116.49)	0
Lin Reg Heavy	8	52	116.65	(116.56, 116.73)	3
Lin Reg Heavy	10	52	116.26	(116.11, 116.41)	3
Log Reg	5	9	-250.76	(-250.76, -250.75)	3
Log Reg	8	9	-250.65	(-250.75, -250.64)	2
RealNVP					
	#LAYER	#HIDDEN	MEDIAN	IQR	#NAN
Poiss Reg	3	16	82576.87	(82575.57, 82577.53)	1
Poiss Reg	5	16	82580.77	(82580.13, 82583.72)	2
Poiss Reg	8	16	N/A	N/A	5
Student t Reg	5	4	-145.52	(-145.53, -145.51)	0
Student t Reg	10	4	-145.52	(-145.52, -145.49)	0
RealNVP					
	#LAYER	#HIDDEN	MEDIAN	IQR	#NAN
Sparse Reg	5	10	-126.33	(-126.36, -126.32)	0
Sparse Reg	8	10	-126.35	(-126.36, -126.33)	1
Sparse Reg High Dim	5	20	-531.75	(-533.41, -522.60)	0
Sparse Reg High Dim	8	20	N/A	N/A	5

Table 2: Comparison of ELBO between ErgFlow and PlanarFlow with different number of layers on real data example. Each setting of PlanarFlow is run in 5 trials. ELBOs of ErgFlow are estimated using 1000 independent trajectories and ELBOs of PlanarFlow are estimated using 2000 independent samples.

ErgFlow					
	STEPSIZE	#LEAPFROG	#REFRESHMENT	ELBO	#SAMPLE
Lin Reg	0.0005	30	2000	-429.98	1000
Lin Reg Heavy	2.50E-05	50	2500	117.1	1000
Log Reg	0.002	50	1500	-250.5	1000
Poiss Reg	0.0001	50	2000	82576.9	1000
Student t Reg	0.0008	80	2000	-145.41	1000
Sparse Reg	0.001	30	600	-125.9	1000
Sparse Reg High Dim	0.0012	50	2000	-538.36	2000
PlanarFlow					
	#LAYER	MEDIAN	IQR	#NAN	
Lin Reg	5	-434.73	(-435.01, -434.65)	0	
Lin Reg	10	-438.79	(-439.25, -436.77)	0	
Lin Reg	20	-442.4384675	(-444.64, -440.93)	0	
Lin Reg Heavy	5	79.65	(-75.92, 99.10)	0	
Lin Reg Heavy	10	23.13	(21.29, 100.10)	0	
Lin Reg Heavy	20	-879.1909019	(-1641.19, -392.80)	0	
Log Reg	5	-251.71	(-251.85, -251.41)	0	
Log Reg	10	-251.8	(-252.03, -251.80)	0	
Log Reg	20	-252.0937812	(-252.20, -251.93)	0	
PlanarFlow					
	#LAYER	MEDIAN	IQR	#NAN	
Poiss Reg	5	82569.58	(82569.33, 82569.68)	0	
Poiss Reg	10	82568.49	(82568.12, 82569.57)	0	
Poiss Reg	20	82566.40441	(82552.57, 82568.05)	2	
Student t Reg	5	-145.69	(-145.71, -145.64)	0	
Student t Reg	10	-145.72	(-145.73, -145.69)	0	
Student t Reg	20	-145.7579931	(-145.77, -145.72)	0	
PlanarFlow					
	#LAYER	MEDIAN	IQR	#NAN	
Sparse Reg	5	-127.58	(-127.60, -127.42)	0	
Sparse Reg	10	-127.75	(-127.87, -127.68)	0	
Sparse Reg	20	-127.6677415	(-128.48, -127.65)	0	
Sparse Reg High Dim	5	-571.97	(-572.09, -565.10)	0	
Sparse Reg High Dim	10	-571.7	(-573.22, -565.55)	0	
Sparse Reg High Dim	20	-577.1338885	(-580.30, -569.39)	0	

Table 3: Comparison of ELBO between ErgFlow and RadialFlow with different number of layers on real data example. Each setting of RadialFlow is run in 5 trials. ELBOs of ErgFlow are estimated using 1000 independent trajectories and ELBOs of RadialFlow are estimated using 2000 independent samples.

ErgFlow					
	STEPSIZE	#LEAPFROG	#REFRESHMENT	ELBO	#SAMPLE
Lin Reg	0.0005	30	2000	-429.98	1000
Lin Reg Heavy	2.50E-05	50	2500	117.1	1000
Log Reg	0.002	50	1500	-250.5	1000
Poiss Reg	0.0001	50	2000	82576.9	1000
Student t Reg	0.0008	80	2000	-145.41	1000
Sparse Reg	0.001	30	600	-125.9	1000
Sparse Reg High Dim	0.0012	50	2000	-538.36	2000
RadialFlow					
	#LAYER	MEDIAN	IQR	#NAN	
Lin Reg	5	-434.14	(-434.36, -434.12)	0	
Lin Reg	10	-434.12	(-434.19, -434.12)	0	
Lin Reg	20	-433.82	(-434.21, -433.73)	0	
Lin Reg Heavy	5	111.99	(111.91, 112.01)	0	
Lin Reg Heavy	10	111.99	(111.89, 112.00)	0	
Lin Reg Heavy	20	111.7	(111.61, 111.71)	0	
Log Reg	5	-251.33	(-251.49, -251.31)	0	
Log Reg	10	-251.17	(-251.21, -251.06)	0	
Log Reg	20	-250.96	(-250.97, -250.95)	0	
RadialFlow					
	#LAYER	MEDIAN	IQR	#NAN	
Poiss Reg	5	82570.5	(82570.19, 82570.57)	0	
Poiss Reg	10	82571.02	(82570.76, 82571.05)	0	
Poiss Reg	20	82571.08	(82570.90, 82571.12)	0	
Student t Reg	5	-145.61	(-145.62, -145.61)	0	
Student t Reg	10	-145.59	(-145.60, -145.59)	0	
Student t Reg	20	-145.58	(-145.60, -145.57)	0	
RadialFlow					
	#LAYER	MEDIAN	IQR	#NAN	
Sparse Reg	5	-127.28	(-127.37, -127.27)	0	
Sparse Reg	10	-127	(-127.03, -126.88)	0	
Sparse Reg	20	-126.68	(-126.69, -126.61)	0	
Sparse Reg High Dim	5	-548.05	(-548.54, -547.98)	0	
Sparse Reg High Dim	10	-547.2	(-547.74, -547.16)	0	
Sparse Reg High Dim	20	-547.03	(-547.78, -546.76)	0	

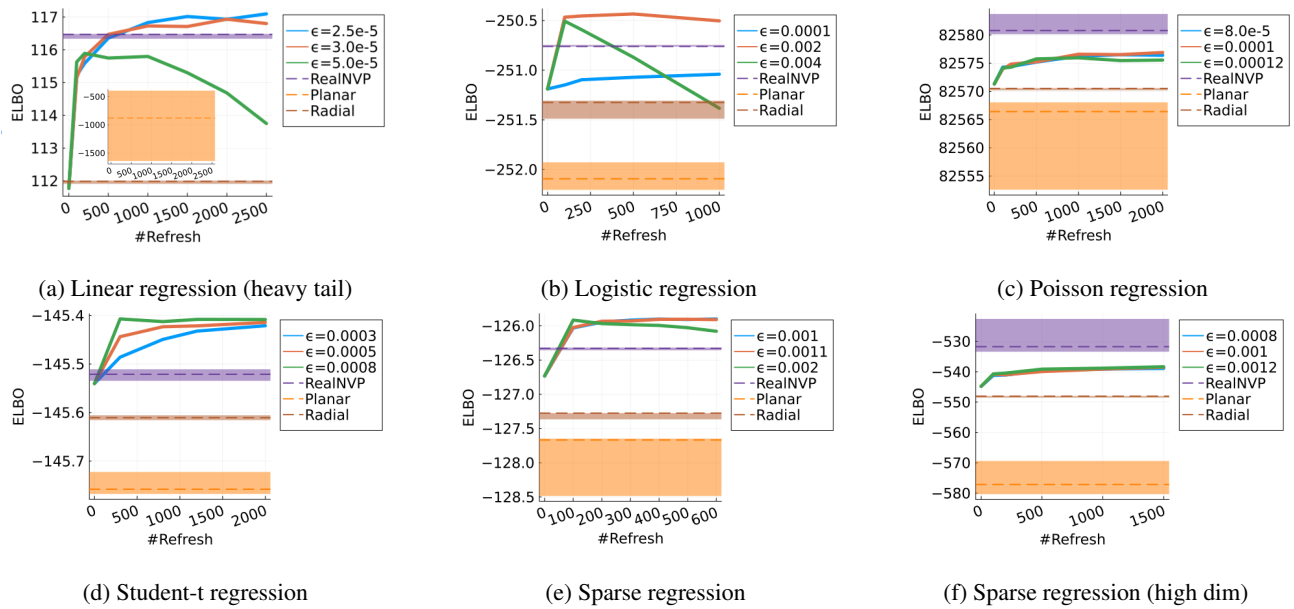


Figure 14: ELBO comparison against NFs for real examples (except for linear regression, which is displayed in Fig. 3a. Each NF method is tuned under various settings, and only the best one is present for each example. Each figure also shows the effect of step sizes on ErgFlow; overly large or small step sizes influence the performance of ErgFlow negatively. Lines indicate the median, and error regions indicate 25th to 75th percentile from 5 runs.

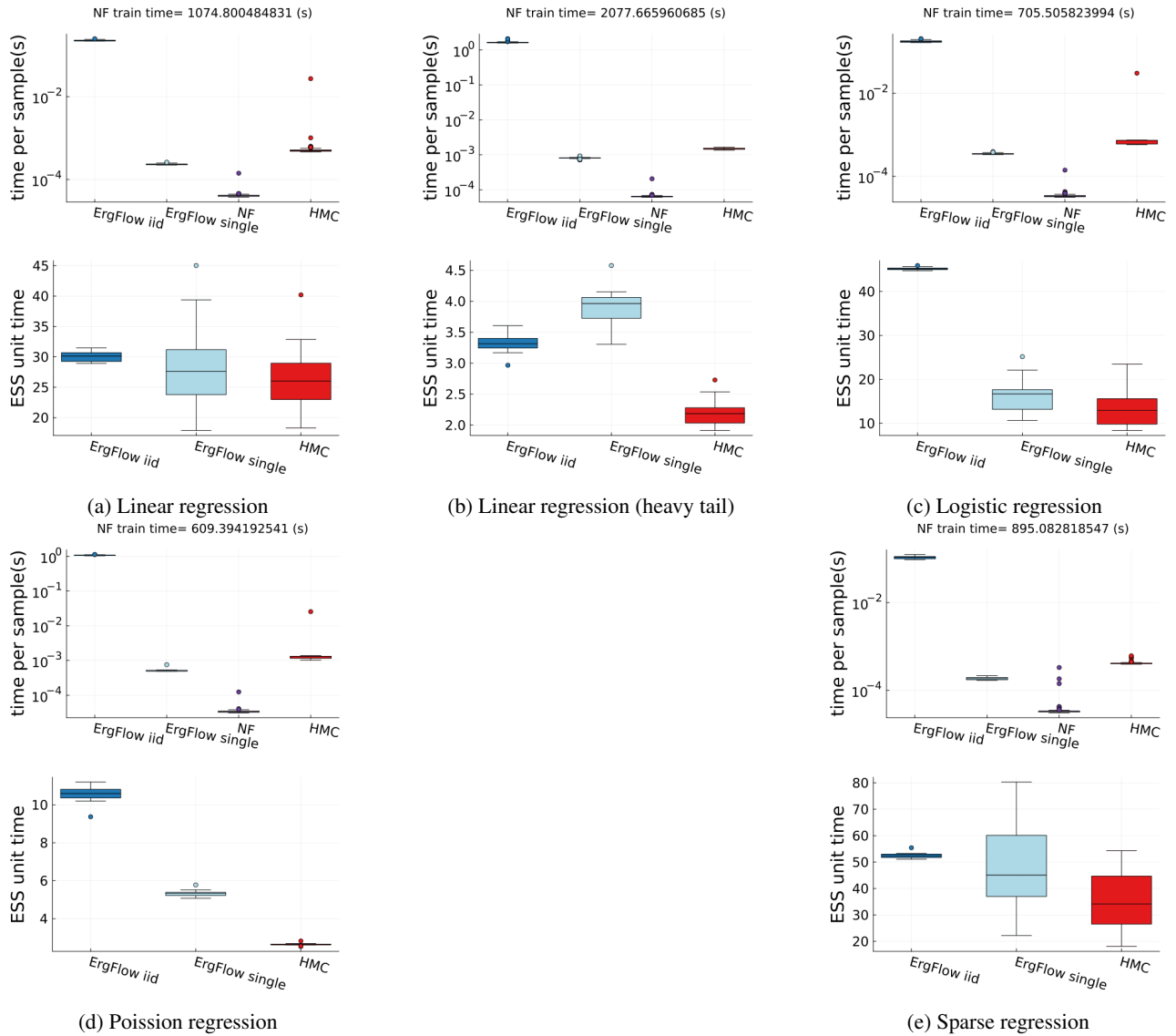
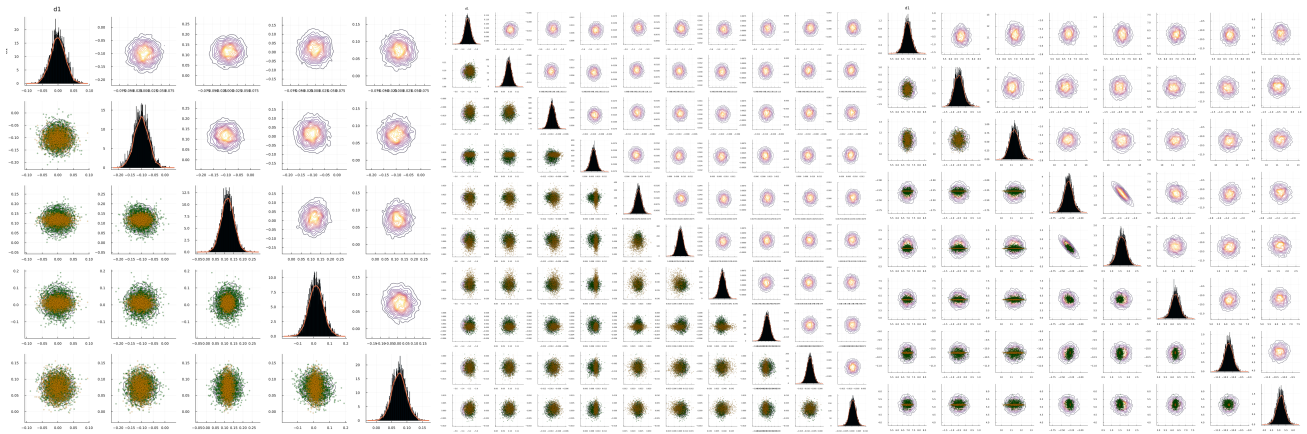


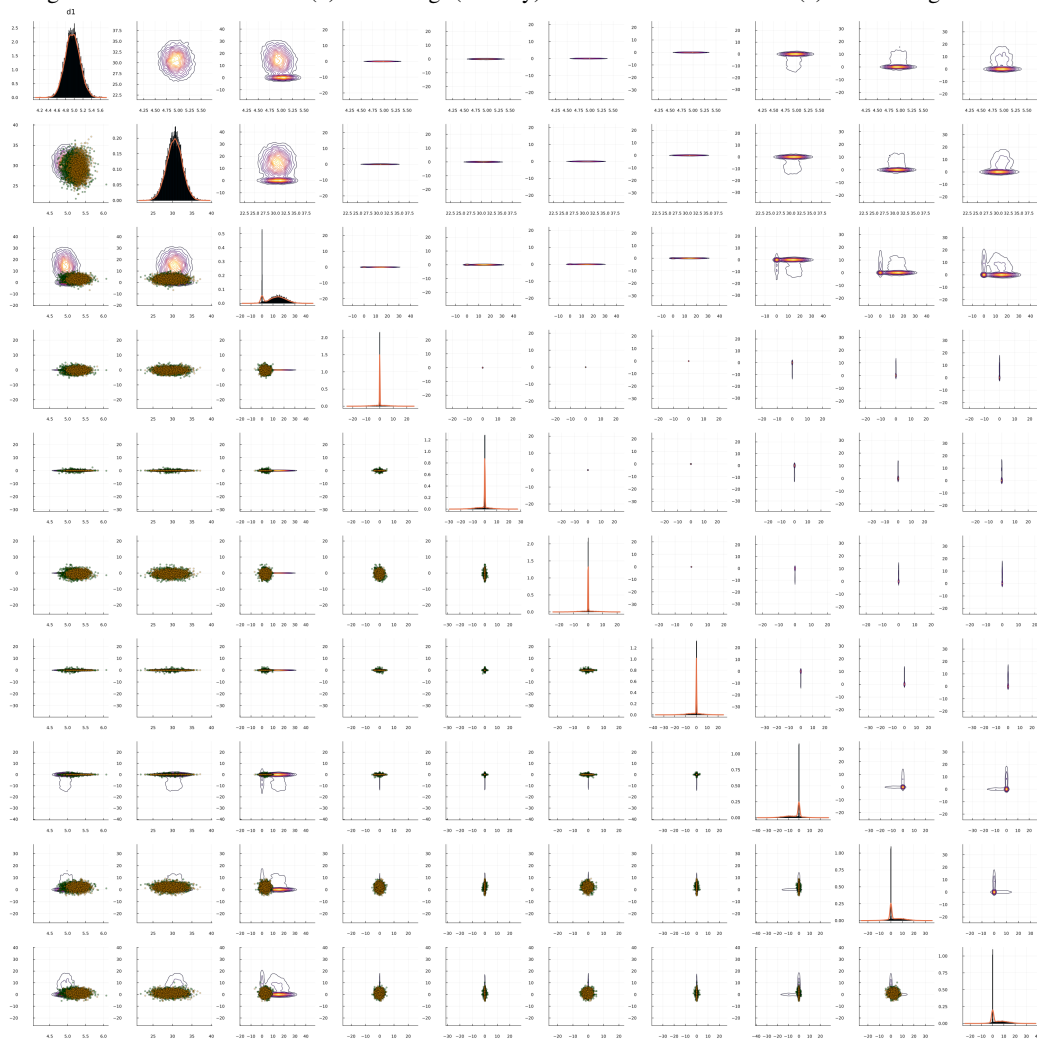
Figure 15: Time results (sampling time comparison to NF, NUTS, and HMC, and per second ESS comparison to HMC; each repeated 100 trials) for two linear regression problems (Figs. 15a and 15b), two generalized linear regression problems (Figs. 15c and 15d), and one sparse regression problem (Fig. 15e).



(a) Linear reg.: first 5 dimensions

(b) Linear reg. (Cauchy): first 10 dimensions

(c) Poisson reg.: all 8 dimensions



(d) Sparse reg. (high dim): first 10 dimensions

Figure 16: Sample quality visualization of 2,000 i.i.d. samples draw from each of ErgFlow (green scatters) and NF (orange scatters) on 4 real data examples: linear regression, linear regression with heavy tail prior, poisson regression, and high-dimensional sparse regression. Pairwise kernel density estimation (KDE) is based on 20,000 NUTS samples, which is initialized with the Gaussian mean of the mean-field Gaussian approximation to posterior distribution, uses 20,000 steps for adaptation (targeting at an average acceptance rate 0.7). NF is chosen to be the same one as compared in Figs. 5 and 15.